Production and Detection of H Atoms and Vibrationally Excited H2 Molecules in CVD Processes

Production and Detection of H Atoms and Vibrationally Excited H_2 Molecules in Chemical Vapor Deposition Processes

By Hironobu Umemoto

Faculty of Engineering, Shizuoka University, Johoku, Naka, Hamamatsu, Shizuoka 432-8561, Japan

E-mail: thumemo@ipc.shizuoka.ac.jp

Radical species, including atomic hydrogen, play an important role in the chemical vapor deposition (CVD) processes to prepare high-quality thin solid films. Detailed information on the absolute densities of these radicals under various conditions is needed in order to understand the chemical kinetics involved and to control the deposition processes. This article reviews the production mechanisms and the gas-phase diagnostic techniques for H atoms in catalytic CVD (also called hot-wire CVD) and plasma-enhanced CVD processes. Experimentally determined absolute H-atom densities in typical CVD processes are compiled in a table. Under suitable conditions, the steady-state H-atom density can be increased up to 10^{17} cm^{-3}. Procedures for producing and detecting vibrationally excited H_2 molecules, which can be another active species in CVD processes, are also discussed.

Keyword: H atoms, H_2 molecules, CVD processes, Laser spectroscopy, Mass spectrometry

1. Importance of H Atoms in Chemical Vapor Deposition Processes

In many low-pressure chemical vapor deposition (CVD) processes, various kinds of free radicals, such as H, CH_3, and SiH_3, are produced and contribute to the deposition and etching. The growth rate and the film properties, such as surface morphology and crystallinity, depend critically on the density and the composition of radical species in the gas phase. Among these radicals, atomic hydrogen is one of the key species.

In this review, techniques for the production and detection of H atoms in CVD processes are discussed. As is always true in this kind of review, it is necessary to limit the scope, since the research area of CVD processes is extremely wide. The author has chosen to focus on experimental studies of catalytic CVD (also known as hot-wire CVD or hot-filament CVD) and plasma-enhanced CVD

employing electric glow discharges. Processes in flame and arc plasma are not included. Simulation or modeling studies are referred to only when necessary. Special attention was paid to the deposition of diamond films and silicon related films, such as hydrogenated microcrystalline silicon. Of course, basic studies related to these CVD processes, such as H-atom detection in pure H_2 systems, are included. The principle and the recent applications of catalytic CVD can be found in References 1-3.[1-3]

The importance of H atoms in the deposition of diamond films with microwave plasma-enhanced CVD has recently been reviewed by Butler et al.[4] The growth mechanism and the roles of H atoms in the CVD processes can be summarized as follows:

1. Gas-phase reactions are initiated by abstracting H atoms from stable source gas species, such as CH_4, to produce radical species, which can react with the vacant surface sites to construct an atomically ordered diamond structure. Although the rate constant for the reaction of $H + CH_4 \rightarrow H_2 + CH_3$ is small at low temperatures because of its large activation energy, 58 kJ mol^{-1}, it becomes large enough at high temperatures, over 1000 K.[5,6]
2. Surface-terminating H atoms are abstracted from the substrate surfaces to create vacant sites for reactions with radical species.
3. Reconstruction to graphite is prevented by terminating the dangling bonds on the surfaces.
4. Carbon sites with sp or sp^2 character are converted into sp^3.

In addition to the creation of radical sites, H atoms may also terminate the vacant sites on the growing surfaces. During such exchange processes of H atoms, the dehydrogenation of adsorbed carbon species and the incorporation of carbon atoms into lattice may take place. Besides the processes presented above, the preferential etching of deposited non-diamond carbon,[7-10] as well as the suppression of the formation of aromatic species in the gas phase,[11] has been demonstrated. It should also be noted that H atoms can be used to clean the substrate surfaces before deposition.[12] The situation should be similar in catalytic CVD processes to prepare diamond films.

A detailed discussion on the roles of H atoms in the deposition of hydrogenated microcrystalline silicon in plasma-enhanced CVD has been given by Matsuda.[13-15] It has been shown that the crystal size as well as the crystalline volume fraction increases with the increase in the

hydrogen-dilution ratio, suggesting the importance of atomic hydrogen in the crystallization. Figure 1 illustrates the substrate temperature dependence of the crystalline volume fraction at three dilution ratios. The crystallinity increases with the increase in the dilution ratio. The sharp decrease in the fraction over 700 K suggests that the surface-hydrogen coverage is essential in the crystalline formation. In order to explain these phenomena, Matsuda introduced three models: etching, chemical annealing, and surface diffusion models.

The etching model was proposed based on the result that the film growth rate decreases by the addition of hydrogen. H atoms reaching the growing surfaces may break weak Si-Si bonds involved in the amorphous structure, leading to a removal of such weakly bonded Si atoms. The vacant site produced is replaced with a new film precursor giving rise to a crystalline structure. However, this preferential etching of weakly bonded Si atoms may not be essential, since no remarkable reduction of film thickness was observed during the hydrogen-plasma treatment in layer-by-layer deposition processes. The chemical annealing model was proposed to explain the formation of microcrystalline silicon in the layer-by-layer growth produced by an alternating sequence of thin amorphous film growth and atomic hydrogen treatment. In this model, H atoms are assumed to permeate through the subsurface to crystallize the amorphous Si network without significant removal of Si atoms. In the surface diffusion model, it is assumed that sufficient flux density of atomic hydrogen results in full surface coverage by bonded hydrogen. H atoms cause local heating through hydrogen-recombination reactions on the film-growing surfaces. These enhance the surface diffusion of film precursors, such as SiH_3. Film precursors adsorbed on the growing surface move to find energetically favourable sites, leading to the formation of a crystallized structure. Local heating may also play a role in diamond deposition,[9,16] but it can be more important in the deposition of silicon-related films, since the typical substrate temperature is rather low in silicon deposition (between 600 and 800 K). The temperature for diamond growth is typically over 1000 K. The lower substrate temperatures are necessary to retain the quality of silicon related films.[14] The importance of the local heating was also confirmed by an experimental work carried out by using D_2/SiH_4 mixtures. It was found that the crystallinity increases with the content of D atoms in the deposited films. This indicates that D atoms reaching the growing surfaces abstract surface-covering bonded H atoms to form HD and also terminate the Si-dangling

bonds. Both these abstraction and recombination processes are highly exothermic and may induce local heating. With regard to gas-phase reactions, since Si-H bonds are much weaker than C-H bonds, radical production processes such as $H + SiH_4 \rightarrow H_2 + SiH_3$ should take place more easily compared to those in diamond deposition. The above reaction to produce SiH_3 may even take place at room temperature.[17]

The situation should be similar in catalytic CVD for fabricating silicon related films. The crystalline fraction increases with the increase in the H_2 fraction in H_2/SiH_4 systems.[1,18] In addition, amorphous silicon can be crystallized by exposure to the H atoms produced by catalytic decomposition.[19,20] Umemoto et al. have shown that the H-atom density in the gas phase decreases drastically when a small amount of SiH_4 is introduced, and that this cannot be explained only by the gas-phase reactions, such as $H + SiH_4 \rightarrow H_2 + SiH_3$. It was necessary to assume that H atoms are removed on the growing surfaces, suggesting the presence of etching and local heating.[21] In the catalytic CVD of $SiH_4/CH_4/H_2$ mixed systems, the incorporation ratio of carbon into the film increases with the increase in the H_2 dilution ratio.[18] This has been explained by the preferential etching of Si compounds by H atoms. Similar results have been obtained in $SiH_4/C_2H_2/H_2$ mixed systems.[22] The properties of SiN_x films can be improved by the addition of H_2 to SiH_4/NH_3 mixtures.[23-27] The etching rate of the deposited films decreases while the breakdown electric field increases. Near perfect conformal coverage can also be obtained on nano-scaled features. These improvements may be ascribed to the extraction of H atoms from the growing surfaces, local heating which induces the radical migration on the substrates, and the activation of catalyst surfaces leading to the increase in the decomposition efficiency of NH_3, which will be discussed just below.

One important role of H atoms specific to catalytic CVD is the re-activation of the catalysts. It has been shown that the decomposition efficiency of NH_3 on heated W surfaces decreases with the introduction of a small amount of SiH_4.[28] This can be explained by the poisoning of the catalyst surfaces by SiH_4. The decomposition efficiency of NH_3, however, recovers with the addition of H_2 as is illustrated in Figure 2.[29] In other words, catalyst surfaces poisoned by SiH_4 can be re-activated by H atoms produced from H_2. Re-activation also can be observed in H_2/O_2 systems.[30,31] In pure O_2 systems, heated W is oxidized rapidly. This oxidization can be suppressed by adding an excess

amount of H_2, and catalytic decomposition can be used to produce O atoms and OH radicals. In this case, atomic hydrogen on W surfaces may eject oxygen, thus preventing oxidization. A similar mechanism to remove adsorbed carbon compounds from catalyst surfaces has also been proposed in H_2/hydrocarbon systems.[32,33]

2. Production Mechanisms for H Atoms

There are many techniques for producing ground-state H atoms, H(1s ^{2}S), including direct photodissociation[34] and mercury photosensitization.[35,36] Very high-density H atoms can be obtained in arc plasma.[37,38] However, when we restrict the discussion to film deposition, especially large-area deposition, glow discharge plasma and catalytic CVD (hot-wire CVD) techniques should be the most practical.

2.1. Glow-discharge Plasma Processes

In discharge plasma, there are many ways to produce H atoms, including direct excitation to repulsive or predissociative states by electron bombardment:

$$H_2 + e^- \rightarrow H_2^* + e^- \rightarrow 2H + e^-,$$

decomposition after ionization and charge recombination:

$$H_2 + e^- \rightarrow H_2^+ + 2e^-,$$

$$H_2^+ + e^- \rightarrow 2H,$$

and dissociative ionization:

$$H_2 + e^- \rightarrow H^+ + H + 2e^-.$$

In the presence of rare gas atoms, Rg, sensitized decomposition may take place:

$$Rg^* + H_2 \rightarrow Rg + 2H.$$

H atoms may also be produced via H^- ions:

$$H_2 + e^- \rightarrow H + H^-,$$

$$e^- + H^- \rightarrow H + 2e^-,$$

or via H_3^+ ions:

$$H_2^+ + H_2 \rightarrow H_3^+ + H,$$

$H_3^+ + e^- \rightarrow H_2 + H.$

The relative importance of these processes will depend on the discharge conditions.

Besides ground-state H atoms, electronically excited species are produced in plasma processes, but most of them are short-lived and decay radiatively before reaching the substrate surface. The radiative lifetime of H(2s ^{2}S) is as long as 0.12 s,[39] but this metastable excited state should be rapidly relaxed by collisional processes to near-by short-lived H(2p ^2P_J) states under medium or low vacuum conditions. Another metastable, $H_2(c\ ^3\Pi_u)$,[40] must be quenched rapidly by H_2 to produce two H atoms, because its electronic energy is much higher than the H-H bond energy. In short, electronically excited species may contribute to gas-phase kinetics, but should not play any role in surface processes.

2.2. Catalytic CVD Processes

The production of ground-state H atoms from H_2 on heated metal surfaces has been recognized since the early 20th century.[41-43] Langmuir found that the heat loss from W wires in the presence of N_2, Hg, Ar, and CO varied with the wire temperature and could be accurately expressed by an ordinary heat conduction equation, but the heat loss in H_2 increased rapidly at temperatures over 1900 K. From a power consumption analysis, he estimated the degrees of dissociation at various temperatures.

The mechanism for producing H atoms from H_2 on heated metal surfaces has recently been discussed by Comerford et al.[44] The kinetic mechanism includes the dissociative adsorption of H_2 onto two different sites on the metal catalyst surfaces followed by subsequent desorption. The activation energies for adsorption and desorption may be different for different crystal faces. However, taking into account that the metal wires used in CVD processes are polycrystalline, the following simplified adsorption/desorption mechanism may be assumed:

$H_2 + S \leftrightarrow H(ads) + H,$

$H(ads) \leftrightarrow H + S.$

Here, H(ads) represents adsorbed atomic hydrogen and S stands for a vacant site on the metal catalyst.

In the catalytic decomposition of H_2, there is a linear relationship between the logarithm of the gas phase density of H atoms and the reciprocal of the catalyst absolute temperature. One of the typical results is shown in Figure 3. The slope of this linear relationship has been regarded as the

activation energy for the production of H atoms. This apparent activation energy is almost half of the dissociation energy of H_2, 432 kJ mol^{-1}, and its dependence on the catalyst materials is minor, as summarized in Table 1.[21,44-52] This is in contrast to the catalytic decomposition of SiH_4 where the activation energy shows a clear dependence on the filament materials.[53]

The agreement between the apparent activation energy and half of the bond dissociation energy of H_2 leads us to assume complete equilibration between H_2 and H. The main role of the filament should be to provide an efficient means by which H_2 molecules can attain the filament temperature;[10,21,47]

$H_2 \leftrightarrow 2H$.

A simple thermodynamic consideration shows that when the temperature dependence of the partition functions is ignored, the steady-state density of H atoms in the gas phase, [H], should be proportional to $[H_2]^{1/2} \exp(-E_{H2}/2RT)$ under complete equilibrium. Here, E_{H2} is the bond dissociation energy of H_2, R is the gas constant, and T is the absolute catalyst temperature. When the decomposition efficiency is small and $[H_2] \gg [H]$, $[H_2]$ may be replaced by the total pressure. Experimentally observed pressure dependence is in accordance with this expectation. The steady-state density of H atoms in the gas phase increases in proportion to the square root of the H_2 pressure, at least below 8 Pa.[21] This view, however, may be too simplistic. It should be noted that the translational temperature of H atoms, even when extrapolated to zero-distance from the filament, is lower than the catalyst temperature.[47,54,55] As will be discussed in Section 6, the vibrational temperature of H_2 is also lower than the filament temperature. Instead of the complete equilibrium model, Comerford et al. have presented a model calculation with adjustable rate parameters for the dissociative adsorption and desorption processes described above. They succeeded in reproducing of the catalyst temperature and the H_2 pressure dependences, as well as the power balance, without assuming complete equilibration between H_2 and H.[44]

H atoms can be produced from hydride molecules other than H_2. In catalytic decomposition, the production of H atoms has been confirmed in pure SiH_4,[49,56-59] NH_3,[60] H_2O,[61] and HCN systems.[62] H atoms have also been detected in plasma decomposition processes of pure CH_4 and SiH_4.[63-68]

3. Removal Mechanisms of H Atoms

Radical species, including H atoms, are chemically unstable and are removed rapidly. The residence time of stable gas molecules in a pumped vacuum chamber is typically about 1 s, while the lifetimes of ground-state radical species are in the order of microseconds or milliseconds. Steady-state density is determined by the balance between the formation and the removal rates. In the presence of material species such as SiH_4, H atoms are mainly consumed in the reactions in the gas-phase and on the growing surfaces. In pure H_2 systems, on the other hand, the main removal route is self-recombination on the chamber walls, in the absence of etching. At low pressures, the self-recombination process in the gas phase is slow.[69] This is because a third body is necessary in such recombination processes; without it, H atoms may rebound elastically with each other. Since no deposition is expected in pure H_2 systems, the H atom diffused to the chamber walls should be reflected or recombined with an H atom on the surface to form an H_2 molecule. This can be a typical example of an Eley-Rideal mechanism. Since the surface recombination rate of H atoms on SiO_2 is one order of magnitude smaller than that on stainless steel,[70-72] it is possible to increase the H-atom density in the gas phase by coating the stainless-steel chamber walls with SiO_2 films. SiO_2 coating can easily be carried out by the oxidation of perhydropolysilazane.[73]

As a result of the recombination processes on chamber walls, there is a gradient in the H-atom density in the gas phase, even in the absence of etching loss. The information on this spatial distribution is also important for simulating the chemical processes taking place in the vacuum chamber. In this sense, spatial resolution is one of the key factors in selecting a detection technique, together with the capability for absolute-density determination, the applicable detection range, and non-invasiveness. For the spectroscopic detection used in plasma processes, distinguishability between the signal and the background emission is also important.

4. Experimental Techniques to Detect H Atoms in the Gas Phase

In situ and non-intrusive detection of radical species, such as atomic hydrogen, is essential for understanding the deposition mechanisms in CVD processes and for the construction of kinetic models.

Laser spectroscopic and mass spectrometric techniques are two of the major techniques to detect atomic hydrogen. Several excellent reviews of laser spectroscopic techniques for gas-phase diagnoses are available.[74-77] Before discussing the merits and limitations of these laser techniques, two conventional techniques, optical emission and resonance absorption techniques, will be briefly reviewed.

4.1. Optical Emission Spectroscopy

Optical emission spectroscopy (OES) is one of the most sensitive, non-invasive, simple, and direct ways to identify radical species.[78-81] Great care, however, must be taken in quantitative analysis. The production of H atoms can easily be identified by Balmer-α (656.3 nm) or Balmer-β (486.1 nm) emission in plasma processes, but the information provided by this technique is for the population of electronically excited species; the population of the ground-state species is not necessarily proportional to that of the excited species, especially when dissociative excitation, such as $H_2 + e^- \rightarrow H(1s\ ^2S) + H(3d\ ^2D_J) + e^-$, is dominant.[82-84] It should also be noted that the emitting species are short-lived and cannot contribute to the surface processes, such as deposition and etching. Optical emission spectroscopy is not applicable to catalytic CVD systems, since no electronically excited species are produced.

4.2. Resonance Absorption

Ground-state H atoms can be detected by resonance absorption using a conventional light source. If the spectral profiles of the light source and the absorption are known, it is possible to evaluate the absolute column densities from the optical transmittance. It should be noted that the simple Beer-Lambert law cannot be applied, since the spectral width of the light source is usually comparable to that of absorption. Numerical calculations are necessary to evaluate the densities from the transmittance. In usual CVD processes, the gas pressure is rather low, below 1 kPa, and pressure broadening of the spectral lines is minor compared to Doppler broadening. Then, the absorption spectral profiles can be represented by Gaussian functions and can be estimated if the temperature of the system is known. The maximum absorption coefficient of the Doppler broadened absorption

profile can be calculated from the wavelength, the radiative lifetime of the upper state, and the ratio of the degeneracy factors of the upper and the lower states.[85] In the case of Lyman-α absorption at 121.6 nm (in this article, wavelengths in the ultraviolet and vacuum ultraviolet regions are those in vacuum), the radiative lifetime of the upper state, $H(2p\ ^2P_J)$, is 1.60 ns.[86] Lyman-α is a doublet and consists of two spectral lines, but this can easily be taken into account in the numerical calculation. The problem is how to evaluate the spectral profile of the light source, because that is often affected by self-absorption effects.[75] Takashima et al. avoided this difficulty by using a high-pressure microdischarge hollow-cathode lamp,[87] and have succeeded in determining absolute densities in many systems by employing this technique.[84,87-89] One limitation in this approach is the narrow dynamic range. Another is the lack of spatial resolution. Information only on the column density can be obtained, unless a special microprobe assembly is used.[89] These limitations are common to the vacuum-ultraviolet laser absorption technique, which will be discussed in Section 4.3.1. The third problem is the background absorption of Lyman-α caused by molecular species such as CH_4 and SiH_4. This problem can be avoided by measuring the absorption of the resonance triplets of N atoms around 120.0 nm as far as the absorption is broad and structureless,[88] but real-time measurement is difficult.

4.3. Laser Spectroscopic Techniques

There are many variations in the laser spectroscopic techniques used to detect ground-state H atoms. The virtues and limitations of typical spectroscopic techniques are summarized in Table 2. Figure 4 schematically illustrates the principles of the spectroscopic techniques introduced in this review.

4.3.1. Vacuum-ultraviolet Laser Absorption Technique

Vacuum-ultraviolet (VUV) laser absorption at 121.6 nm is one of the most common techniques.[21,30,50,52,73,90-94] The procedure to produce VUV laser radiation will be discussed in Section 4.3.7. The principle of this technique is the same as that of resonance absorption and the data analysis procedure is also the same. The difference is that a laser is used instead of a conventional light source. In this case, it is not necessary to take self-reversal effects into account. When the spectral profile of

the laser can be represented by a Gaussian function, the transmittance is given by the following equation:

$$T(\omega_L) = \frac{\int_0^\infty \exp\left\{-\left(\frac{\omega-\omega_L}{\alpha}\right)^2\right\} \exp\left\{-k_0 l \exp\left(-\left(\frac{\omega-\omega_0}{\beta_0}\right)^2\right) - k_1 l \exp\left(-\left(\frac{\omega-\omega_1}{\beta_1}\right)^2\right)\right\} \mathrm{d}\omega}{\int_0^\infty \exp\left\{-\left(\frac{\omega-\omega_L}{\alpha}\right)^2\right\} \mathrm{d}\omega}.$$

Here, α, β_0, and β_1 are parameters that represent the spectral width of the light source and the absorption, respectively. There are two components for absorption since Lyman-α is a doublet. The subscripts 0 and 1 stand for the transitions to 2p $^2P_{1/2}$ and 2p $^2P_{3/2}$, respectively. The central angular frequency of the light source is represented by ω_L, while ω_0 and ω_1 are the angular frequencies at the absorption peaks. The absorption coefficients at the Doppler-broadened line centers are represented by k_0 and k_1, while l is the absorption path length. It is assumed that the laser is weak enough not to cause stimulated emission. The values of β_0, β_1, k_0, and k_1 are given by:

$$\beta_0 = \left(\frac{2kT}{m}\right)^{1/2} \frac{\omega_0}{c},$$

$$\beta_1 = \left(\frac{2kT}{m}\right)^{1/2} \frac{\omega_1}{c},$$

$$k_0 = \left(\frac{m}{2\pi kT}\right)^{1/2} \frac{\pi^2 c^3 N}{\tau \omega_0{}^3},$$

$$k_1 = \left(\frac{m}{2\pi kT}\right)^{1/2} \frac{2\pi^2 c^3 N}{\tau \omega_1{}^3},$$

where m is the mass of H atoms, k is the Boltzmann constant, T is the absolute translational temperature, c is the speed of light, N is the density of ground-state H atoms, and τ is the radiative lifetime of H(2p ^2P_J), 1.60 ns. Figure 5 illustrates typical absorption spectra of H atoms produced by the catalytic decomposition of H_2.

The merit in the absorption technique is, as has been mentioned in Section 4.2, the ability to determine absolute column densities. When a laser is used as a light source, it is easy to scan the wavelength and eliminate the broad background absorption by source and product molecular species.

This method is insensitive to collisional quenching of the upper states and background plasma emission, which can be a problem in laser-induced fluorescence measurements, as will be discussed in Section 4.3.3. The problem is that the dynamic range is rather narrow, unless the path length can be greatly changed. In general, it is hard to measure the absorption to less than 5%. When the intensity of the light source fluctuates, the sensitivity decreases even further. The uncertainty is large when the absorption is more than 90%. When the path length is 10 cm, the dynamic range is restricted to the order of 10^{11} cm^{-3}.

A combination of a vacuum-ultraviolet (VUV) monochromator and a solar-blind photomultiplier tube can be used to evaluate the transmitted laser intensity, while the measurement of the NO^+ ion current is another convenient technique. NO is not ionized by unfocused near UV radiation, such as that at 364.7 nm; the wavelength before frequency tripling to produce Lyman-α. The absorption of Lyman-β (102.6 nm) and Lyman-γ (97.3 nm) radiation has also been used to detect H atoms.[95,96] In such cases, however, differential pumping systems are necessary because the wavelengths are shorter than the cut-off wavelength of LiF, the window material for the shortest wavelengths. Besides lasers, synchrotron radiation can also be used as a narrow-band tunable light source.[97]

4.3.2. One-photon Laser-induced Fluorescence Technique

Laser-induced fluorescence (LIF) techniques, both one-photon and two-photon, are useful to extend the dynamic range. The relative values obtained by LIF techniques can be scaled to absolute values by comparing the signal intensities where absolute values are available. The procedures to evaluate absolute densities, other than absorption techniques, will be discussed in Section 4.5. In one-photon laser-induced fluorescence (vacuum-ultraviolet LIF), laser radiation at 121.6 nm is used to excite ground-state H atoms, H(1s ^2S), to H(2p ^2P_J) states.[30,50,90,91,98] The induced fluorescence is monitored at an angle perpendicular to the laser beam with a solar blind photomultiplier tube. A VUV monochromator is not necessarily required and an interference filter is enough to isolate the fluorescence. Saturation of the signal intensity against the laser intensity, which can often be a problem in one-photon LIF in the visible or near UV regions,[75] cannot be a great problem in this case,

since the efficiency to produce VUV radiation is usually low.[99] In general, the LIF intensity of a two-level system under stationary excitation is given by:

$$I_{LIF} = K \frac{A_{21} g_2 \rho(\omega_0) B_{12} N}{\rho(\omega_0) B_{12} (g_1 + g_2) + A_{21} g_2 + g_2 k_q n_q}.$$

Here, K is the instrumental constant, A_{21} and B_{12} are the Einstein coefficients for spontaneous emission and stimulated absorption, g_1 and g_2 are degeneracy factors of lower and upper levels, $\rho(\omega_0)$ is the energy density of the laser at the angular frequency of ω_0, which is resonant to the energy difference between the two levels, N is the number density of the lower-level species, k_q is the rate constant for the quenching of the upper state, and n_q is the number density of the quenching species. The assumption of a two-level system is valid with regard to the LIF at Lyman-α. The upper two levels may be regarded as one degenerate level. Stimulated emission can usually be ignored compared to the spontaneous emission, since VUV laser radiation is rather weak. Although the rate constant for the quenching of H(2p ^2P_J) by H_2 can be as large as 2.5×10^{-9} cm^3s^{-1},[100] collisional quenching can be ignored when the pressure is lower than 100 Pa, since the radiative lifetime of H(2p ^2P_J) is short. When the H-atom density is high and radiation trapping cannot be ignored, the effect of quenching must be taken into account, but, under such conditions, this technique may not be applicable in any case, as will be discussed below. Then, the first and the third terms in the denominator can be neglected under usual conditions and the above equation can be simplified as follows:

$$I_{LIF} = K \rho(\omega_0) B_{12} N.$$

In short, the LIF signal intensity is directly proportional to the density of ground-state H atoms and the laser intensity. The same relationship can be derived under repeated rectangular pulsed excitations when the time-averaged fluorescence intensity is measured. The VUV LIF technique is more sensitive than the absorption technique, but it cannot be employed when the H-atom density is high because the system becomes optically too thick. For example, when the H-atom density is 5×10^{10} cm^{-3}, the attenuation of the VUV laser beam cannot be ignored when the path length is more than 10 cm.

4.3.3. Two-photon Laser-induced Fluorescence Techniques

H(1s ^2S) can also be two-photon excited to H(2s ^2S).[30] The exciting wavelength should be 243.1 nm. H(2s ^2S) is metastable and does not fluoresce, but it is easy to collisionally relax to the

near-by 2p ^2P_J states, which fluoresce Lyman-α. Like the VUV LIF technique, this technique is also sensitive, but cannot be employed when the H-atom density is high. In this case, the effective radiative lifetime is lengthened by radiation trapping and it becomes necessary to take into account the effect of the quenching of the upper state. This correction is not straightforward without a direct lifetime measurement, which is usually difficult. When quenching cannot be ignored, the quantum yield of the fluorescence should depend on the imprisoned lifetime, which is a function of the H-atom density. In short, it is necessary to know the H-atom density so that it can be evaluated. It is also possible to two-photon excite H(1s ^2S) to H(2s ^2S) at 243.1 nm, and then one-photon excite to a higher state, such as H(3p ^2P_J) and H(4p ^2P_J).[67,101] In these cases, it is possible to observe Balmer-α or Balmer-β radiation, although photon release via the Lyman series is more efficient. It should also be noted that these two-photon excitation techniques at 243.1 nm, together with the (2+1) resonance-enhanced multiphoton ionization technique discussed in Section 4.3.5, are the best for measuring the Doppler profiles, from which information on the translational temperature can be obtained.[47,55,102] This is because the upper state, H(2s ^2S), is not split as for H(2p ^2P_J) and there are no fine structures. The spin-orbit splitting for H(2p ^2P_J) is as small as 0.365 cm^{-1} and the Lyman-α lines corresponding 2p $^2P_{3/2}$ – 1s $^2S_{1/2}$ and 2p $^2P_{1/2}$ – 1s $^2S_{1/2}$ transitions cannot be resolved at moderate temperatures.

Another two-photon laser-induced fluorescence technique following excitation at 205.1 nm can be used to detect high-density H atoms at more than 10^{13} cm^{-3}.[21,30,50,52,54,63-66,70,76,82,94,103-119] In this case, H(1s ^2S) is excited to H(3s ^2S) and H(3d ^2D_J) states and Balmer-α emission at 656.3 nm is monitored. This technique is less sensitive, but can be used in the presence of an excess amount of H atoms since radiation trapping is not expected in this visible transition. Here, since no VUV radiation is used, either in excitation or detection, it is not necessary to account for the effects of VUV absorption by molecular species, such as CH_4 and SiH_4. It is also possible to determine the absolute densities by measuring the two-photon LIF signal intensity of a known amount of Kr following excitation at 204.2 nm.[119,120] Since laser beams are focused in two-photon excitation schemes, it is necessary to ensure the signal intensity is proportional to the square of the laser intensity. When the laser is too intense, there will be a signal loss due to three-photon ionization.

In density measurements by two-photon LIF at 205.1 nm, the quenching processes of the upper states cannot be ignored in the presence of more than 10 Pa of H_2. This is because the radiative lifetimes of H(3s ^{2}S), H(3p ^2P_J), and H(3d ^2D_J) states are much longer (158, 45, and 15 ns, respectively) than that of H(2p ^2P_J),[86] while the rate constants for the quenching of these states are extremely large; the rate constants for H_2 are as large as 2×10^{-9} cm^3s^{-1}.[120-123] In addition, the detection of Balmer-α is sometimes obscured by plasma emission or black-body radiation from the filament. These backgrounds can be reduced by using a monochromator or by setting a short detection time gate, since pulsed lasers are usually used; it is difficult, however, to eliminate them completely. These problems can be avoided by monitoring the amplified spontaneous emission (ASE)[107,114] or by employing two-photon polarization spectroscopy.[124]

4.3.4. Amplified Spontaneous Emission and Two-photon Polarization Techniques

When the H atom density and the laser intensity are high enough to create population inversion between the upper and lower levels, usually between H(3d ^2D_J) and H(2p ^2P_J), ASE can be observed at 656.3 nm after the excitation at 205.1 nm.[107,114] Since ASE is emitted like a laser beam within a small solid angle and is not divergent, this technique can be applied in the presence of intense background emission. This technique is also insensitive to collisional quenching. In two-photon polarization spectroscopy, a circularly polarized pump beam is focused into the detection zone, where it overlaps with a linearly polarized signal beam. In the arrangement of Gonzalo et al.,[124] the wavelength of both beams was 243.1 nm, two-photon resonant to the H(2s ^{2}S-1s ^{2}S) transition. In the presence of H atoms, the polarization of the signal beam is rotated and becomes elliptic. The H-atom density can be evaluated by measuring this polarization change. This technique is not affected by either background emission or quenching. The absolute density can be determined by measuring the non-resonant two-photon polarization signal of Xe.

4.3.5. Resonance-enhanced Multiphoton Ionization Techniques

Resonance-enhanced multiphoton ionization (REMPI) techniques also have been widely used to detect H atoms.[44,47,55,57,58,102,125-128] H(2s ^{2}S) produced by two-photon excitation at 243.1 nm can easily be ionized by absorbing an additional photon. It is not necessary to take into account the effect of quenching. By detecting the ions or electrons produced, it is possible to evaluate the ground-state

H-atom densities. This technique is extremely sensitive when combined with a time-of-flight mass spectrometric technique. For example, it is possible to detect H atoms produced by the non-resonant two-photon dissociation of H_2 under beam conditions.

In multiphoton detection techniques, such as two-photon LIF and REMPI, it is possible to obtain information on spatial distributions. Laser beams are usually focused with a convex lens and multiphoton processes may take place only near the focal point. Thus, information can only be obtained near the focal point. This is in contrast to absorption techniques, with which only information averaged along the optical path can be obtained. The problem is that an intense, focused laser beam may induce photochemical reactions to produce H atoms. In two-photon excitation, especially at 205.1 nm, the multiphoton dissociation of material or product gases, such as NH_3 and Si_2H_6, is hard to avoid and the production of extra H atoms is inevitable.[64,67,109,110,116] The effect of multiphoton decomposition can be reduced by employing lasers with longer wavelengths. It is possible to ionize H atoms by exciting at 364.7 nm.[45,129] In this case, H(1s ^{2}S) is three-photon excited to H(2p ^2P_J) and then ionized. This (3+1) REMPI technique is less sensitive than (2+1) REMPI, but also less intrusive.

4.3.6. Other Laser Spectroscopic Techniques

Third-harmonic generation (THG) is another non-intrusive multiphoton technique used to detect H atoms.[9,130] With this technique, laser beams near 364.6 nm are focused in the chamber and the generated third-harmonic around 121.5 nm is observed. In general, the refractive index increases with the decrease in the wavelength and it is difficult to match the phases of the fundamental and third-harmonic waves. Fortunately, however, a region of negative dispersion exists on the short-wavelength side of a dipole-allowed transition, at 121.6 nm for H atoms, and the third-harmonic wave can be grown monotonically with the optical path. In other words, the efficiency of the third-harmonic generation at a wavelength a little shorter than 121.6 nm is enhanced by the presence of H atoms. The generated third-harmonic intensity is proportional to the square of the H-atom density, while the peak wavelength shift is proportional to the density. The detection sensitivity is rather low, on the order of 10^{13} cm^{-3}, but this technique can be used under high-density conditions because the generated third harmonic is shifted against the resonance radiation and the self-absorption is not significant.

Background emission cannot be a problem since the signal beam is non-divergent along the input laser beam.

In addition to the above, there are a number of other laser spectroscopic techniques to detect H atoms, such as three-photon excitation at 291.8 nm followed by subsequent fluorescence,[131] two-color two-photon LIF following excitation at 193 and 219 nm or 193 and 195 nm,[132] two-color (1'+1) REMPI through excitation at 121.6 and 364.7 nm,[133] two-photon-resonant four-wave-mixing,[134,135] and two-color laser-induced grating spectroscopy.[136] However, these techniques do not appear to have been applied to gas-phase diagnoses in catalytic or plasma-enhanced CVD processes.

4.3.7. Frequency Conversion Techniques

As has been shown, UV or VUV radiation below 364.7 nm is necessary for the spectroscopic detection of H atoms. It is difficult to obtain such UV or VUV radiations directly from tunable lasers; frequency conversion, doubling, tripling, mixing, or shifting is necessary. One exception is a XeCl excimer-pumped dye laser, which can be used to generate the 364.7-nm radiation directly. Techniques to generate tunable short-wavelength radiations for diagnoses have been reviewed by Döbele et al.[74] Radiations at 364.7, 243.1, and 205.1 nm can be obtained using commercial tunable lasers and nonlinear optical crystals such as β-BaB_2O_4 (BBO). Lyman-α radiation at 121.6 nm can be obtained by tripling the laser radiation at 364.7 nm with Kr gas.[99] Addition of Ar is effective for phase matching. Stimulated anti-Stokes Raman scattering in H_2 or D_2 can also be used. Since these frequency conversion efficiencies strongly depend on the peak intensity, nanosecond pulsed lasers are usually used, rather than continuous-wave (CW) lasers. One of the typical choices is a Q-switched Nd:YAG (YAG denotes yttrium aluminum garnet) laser-pumped dye laser. An optical parametric oscillator (OPO) pumped with a Nd:YAG laser also can be used. Excimer pumped dye lasers and Raman-shifted excimer lasers can also be used, but the time jitters are larger than those in YAG systems. Pico- and femto-second lasers are not usually used because of their lack of energy (wavelength) resolution as well as high instrumental costs.

4.4. Mass Spectrometric Techniques

Mass spectrometry is another widely used technique to detect H atoms. This method is molecular unspecific and any atoms and molecules can be detected. This is in contrast to the laser techniques, which are selective and molecular specific and can be both a merit and a disadvantage. Two points should be addressed here. The first is dissociative ionization, such as $H_2 + e^- \rightarrow H^+ + H + 2e^-$. In conventional quadrupole mass spectrometers, the energy of electrons to ionize neutral species is around 70 eV. Such spectrometers are not suitable for radical detection because these high-energy electrons cause fragmentation of the parent molecules to produce ionic species. A threshold ionization technique is used to avoid this dissociative ionization of the source gas molecules, whose densities are much higher than those of radical species.[48,49,56,59,68,71,72,128,137-141] To achieve selective ionization with the threshold ionization technique, the energy of the electrons for ionization is chosen to be higher than the ionization energy of the radical species (for example 13.6 eV for H atoms), but lower than the appearance potential of the dissociative ionization (e.g., 18.1 eV for H_2). Selective ionization is also possible by photoionization. However, in order to photoionize H atoms in a single-photon process, the wavelength must be shorter than 91 nm, which is shorter than the LiF cut-off. The widely used photoionization light source, the 9^{th} harmonic of a Nd:YAG laser at 118 nm, cannot be used here. The second point to be emphasized is that in situ measurements are rather difficult in mass spectrometric techniques. Mass selection must be carried out after ionization and the pressure in the flight tube must be less than 10^{-3} Pa in order to avoid collisions with gas molecules before reaching the detector. This pressure is much lower than the typical pressures in CVD processes. The usual technique is to place a sampling hole between the CVD and the ionization chambers and to differentially pump the ionization chamber.

4.5. Calibration Techniques

Absolute density measurements are desirable in many systems, but it is not always possible to obtain them. Calibration techniques have been developed, therefore, in order to scale the relative values to absolute ones. Besides VUV absorption, titration is one of the most widely used techniques.[66,74,77,98,103,105,106,113,117,118] A discharge flow system is usually used in this technique. H atoms produced by electric discharges of H_2 are mixed with NO_2 at the downstream side of the flow

and are consumed by the H + NO_2 → OH + NO reaction. The H-atom signal decreases linearly with the increase in the NO_2 density until it becomes indistinguishable from the background. The NO_2 density at this end point is equal to the H-atom density at the beginning of the titration. The absolute calibration for one-photon LIF can be carried out by comparing the LIF signal intensities with those of the Rayleigh scattering caused by rare gas atoms, such as Ar.[77,98] Since the absolute differential cross-section for Rayleigh scattering can be calculated from the refractive index, the instrumental constant (i.e., the product of the sensitivity and the solid angle for detection) can be evaluated. In general, induced fluorescence is not isotropic even if the laser is unpolarized, and this anisotropy must be taken into account.[142-144] This correction, however, is not significant for Lyman-α.[98] As has been mentioned in Section 4.3.3, the calibration for two-photon LIF at 205.1 nm can be carried out by measuring the signal intensity of Kr.[119,120]

4.6. Other Conventional Techniques

Finally, some comments should be made on convenient non-spectroscopic techniques to determine H-atom densities. As has been discussed, the H-atom recombination reaction is highly exothermic. Tankala and DebRoy used a catalytic probe constructed with two thermocouples.[16] The tip of one thermocouple was covered with quartz, while the other tip was wrapped with a silver wire. The tip covered with silver is heated more because of the efficient catalytic recombination reactions of H atoms on silver surfaces; thus the relative H-atom density can be evaluated by measuring the temperature difference between the two tips. A similar technique has also been developed by Gardner.[145] Another technique utilizes the reduction reaction of tungsten oxide.[146,147] WO_3 doped in phosphate glass plates can be reduced by exposure to H atoms and the degree of reduction can be evaluated from the change in the optical transmittance. It should be noted that the reduction by H_2 molecules is minor even at elevated temperatures. The absolute densities can be evaluated by calibrating the changes in optical transmittance. Although this technique cannot be used under depositing conditions, no special instruments or skills are required.

5. Experimental Results of H-atom Density Measurements

Table 3 summarizes the absolute steady-state densities of H atoms in the gas phase produced by the catalytic and glow-discharge decomposition of H_2 molecules. The results were restricted to those obtained in pure H_2 or highly H_2-diluted systems. Results obtained in pulsed discharge systems are not included. In Figure 6, the maximum H-atom density reported is plotted as a function of H_2 pressure. H-atom density may depend not only on H_2 pressure but also on the chamber size and wall conditions, since the main removal process of H atoms is that on walls. In addition, in catalytic processes, the H-atom density depends on the temperature and length of the filament. In plasma processes, that depends on the electric discharge power and the frequency. Most importantly, not all investigators have tried to attain the maximum population in their procedures. In spite of these complex situations, Figure 6 shows that the H-atom density can be higher in catalytic decomposition since it is possible to increase the H_2 pressure. This is in contrast to the cases for the production of atomic oxygen and nitrogen. It is possible to produce O and N atoms in catalytic decomposition of pure O_2 and N_2, but their densities are much lower than those in plasma processes, although they can be clean sources of O and N atoms since no metastable excited species, such as $O(2p^4\ ^1D_2)$ and $N_2(A\ ^3\Sigma_u^+)$, are produced.[148,149] N-N bonds may be too strong to be broken easily in catalytic processes. O-O bonds are also stronger than H-H bonds. Since catalytic decomposition is a mild process, the bond energy dependence may appear more strongly. In plasma processes, in addition, decomposition efficiency may decrease with the decrease in the number of outer-shell electrons. In other words, H_2 is the most difficult molecule to decompose by electron bombardment. This explanation is consistent with the results that the H-atom density always decreases with the addition of CH_4 or SiH_4 in catalytic decomposition[21,45,104,137] but increases in some plasma processes.[65,84,88]

6. Production and Detection of Vibrationally Excited H_2 Molecules

6.1. Production of Internally Excited H_2 Molecules

H_2 molecules are not only decomposed but also are rotationally and vibrationally excited by contact with hot metal surfaces or accelerated electrons. Two processes have been proposed for excitation by electrons.[150] One is the so-called *E*-to-*V* process, in which vibrationally excited H_2 is produced via electronically excited H_2. Another is the *e*-to-*V* process. In this process, vibrationally

excited H_2 is produced directly by the collision of low energy electrons. Rotational excitation may, of course, take place simultaneously. In addition, internally excited H_2 should be produced in the H+H recombination reactions on surfaces.[151-153] In general, the reaction rate constant increases with the rotational or vibrational excitation. Especially, the vibrational quantum of H_2 is large and the effect is large. For example, the vibrational excitation of H_2 increases the rate constants for $O(2p^4\ ^3P_J) + H_2$ and $OH(X\ ^2\Pi_J) + H_2$ reactions by more than two orders of magnitude.[154,155]

Rotational relaxation is, in general, rapid. The bimolecular rate constants for the rotational relaxation of H_2 by H_2 have been reported to be on the order of 10^{-11} or 10^{-12} cm^3s^{-1}.[156-159] This value is smaller than those for other diatomic molecules with smaller rotational spacing,[160] but it is still large enough to thermalize rotationally hot H_2 molecules within 100 collisions. This is consistent with the observation that the rotational state distribution is Boltzmann-like in many systems. In other words, it is possible to determine the temperature of the system by measuring the rotational distribution. On the other hand, vibrational distribution is not necessarily Boltzmann-like and the vibrational energy is sometimes much higher than the thermal energy of the system. Then, vibrationally excited species can be another active medium in CVD processes.

In plasma processes, vibrationally highly excited H_2 molecules, up to the vibrational quantum number of 13, have been identified.[161,162] In activation on hot filaments, Hall and coworkers have shown that vibrationally excited states up to v=9 are produced, where v represents the vibrational quantum number.[151,153] It has been shown, however, that the population of these highly excited states is several orders of magnitude smaller than that of ground-state H_2 molecules.[151,153,161-164] The population is also much smaller than the typical population of H atoms. Therefore, the role of these vibrationally highly excited H_2 in CVD processes must be limited. Therefore, the following discussion will be restricted to $H_2(v=1)$.

6.2. Detection of Vibrationally Excited H_2 Molecules

One of the most widely used techniques to determine the vibrational state distributions of H_2 is coherent anti-Stokes Raman scattering (CARS).[9,128,157,165-170] In typical CARS measurements, the second harmonic of a Q-switched Nd:YAG laser at 532 nm is split into two parts. One part is used to

pump a dye laser whose output around 684 nm is used as the tunable Stokes beam, ω_S. The remaining part is used directly as the pump beam, ω_P. Four-wave mixing generates an anti-Stokes signal beam, $\omega_{AS} = 2\omega_P - \omega_S$ around 435 nm. There are two choices to record the CARS spectra. One is to record the intensity of the anti-Stokes signal by scanning the wavelength of the Stokes beam using a high-resolution tunable laser. Another is to record the dispersed spectra of the anti-Stokes signal using a low-resolution tunable laser and a high-resolution detection system. Figure 7 shows a typical example of the former method. In general, the CARS signal intensity is proportional to the square of the third-order nonlinear susceptibility, $\chi^{(3)}$, which is proportional to the difference in the populations of $H_2(v+1)$ and $H_2(v)$ and also depends on v and J, where J is the rotational quantum number. It should be noted that $\chi^{(3)}$ depends little on J, but is proportional to $v+1$. In other words, the detection sensitivity for $H_2(v=1)$ is 4 times larger than that for $H_2(v=0)$. The sensitivity of CARS is low and the spatial resolution is limited, unless BOXCARS or folded BOXCARS arrangements are employed, but absolute calibration is possible since it is easy to detect $H_2(v=0)$. Vibrationally excited H_2 can be detected by LIF[161,163] and absorption spectroscopy.[93,163,164,171] With these techniques, however, it is impossible to detect $H_2(v=0)$, and hence to evaluate the $H_2(v=1)/H_2(v=0)$ population ratio without using short-wavelength radiation below the LiF cut off. H^- ions are formed by the dissociative attachment of electrons to vibrationally excited H_2 molecules and this can be used to determine the vibrational state distributions,[151,153] but sensitivity decreases rapidly with a decrease in the vibrational quantum number. Although excitation around 290 nm followed by (3+1) REMPI can be used to detect the low vibrational states,[129,152,172] charged particles present in the plasma discharge volume may obscure the signals in this technique.

Tables 4 and 5 summarize the rotational temperature and the ratio of the $H_2(v=1)$ population to that of $H_2(v=0)$ in hot-wire and glow discharge excitation. Although the state distributions must depend on the experimental conditions, such as the chamber geometry and total pressure, it can be concluded that the $H_2(v=1)/H_2(v=0)$ population ratio is smaller in hot-wire excitation than in plasma excitation. In other words, vibrationally excited H_2 must be more important in plasma processes. Since the production efficiency of H atoms in catalytic decomposition is often greater than that for

plasma processes, the lower vibrational excitation in hot-wire systems suggests that the H+H recombination is not the main source of $H_2(v=1)$. $H_2(v=1)$ must mainly be formed on the hot wire surfaces or by collisions of H_2 with electrons. It has been suggested that the role of sub-excited electrons, with kinetic energy less than 1 eV, is important in plasma processes.[129,165] According to Shakhatov et al., the vibrational temperature is lower at higher pressures, while an opposite result has been obtained by Umemoto et al.[168-170] These results suggest that collisional relaxation processes in the gas phase and those on chamber walls are competing.[173] Although the rate constant for the vibrational relaxation of $H_2(v)$ by H_2 is small at room temperature,[174-180] that increases rapidly with rising temperature.[178,179,181] The rate constant for the vibrational relaxation by H atoms is large because it may proceed via a chemical atom-transfer process, $H+H_2(v=1) \rightarrow H_2(v=0)+H$,[182,183] which also could contribute to the vibrational relaxation. In spite of the presence of such relaxation processes, $H_2(v=1)$ must have lifetimes long enough to collide with the substrate surfaces. The role of vibrationally excited H_2 in CVD processes is not clear and remains an issue to be resolved.

7. Concluding Remarks

There are three stages in catalytic and plasma-enhanced CVD processes. The first is the production of radical species from source gas molecules. The second is the transportation of these species, in which gas-phase reactions and relaxations may take place. The final stage is the deposition of the film precursors on the substrate surfaces. Etching and surface recombination processes should also be important. Reactive radical species, including atomic hydrogen, play key roles not only in the gas phase, but also in the final step on the growing surfaces, but it is still hard to identify the radical species adsorbed on surfaces. Many surface analysis techniques, which utilize ions and electrons, are difficult to apply, since CVD processes are usually carried out in low or medium vacuum. Herein lies the importance of gas-phase diagnoses.

There are many techniques to identify H atoms in the gas phase, but none of them are all-encompassing. In order to elucidate the detailed chemical kinetics, many techniques must be combined. Fortunately, the roles of H atoms in simple systems, such as pure H_2 and CH_4/H_2 mixed systems, are becoming fairly clear. It is still hard, however, to prospect the roles in complex systems,

such as $SiH_4/CH_4/H_2$ and $SiH_4/NH_3/H_2$ systems. Besides these, diagnoses in systems to prepare extrinsic semiconductor films, such as $CH_4/B_2H_6/H_2$ and $SiH_4/PH_3/H_2$ systems, should be important and can be the research targets in the next decade. In $CH_4/B_2H_6/H_2$ systems, the B-atom density is estimated to be higher than those of BH, BH_2, and BH_3, due to the rapid H-shifting reactions, $BH_x + H \rightarrow BH_{x-1} + H$ ($1 \leq x \leq 3$), in modelling studies.[127,184] Similar efficient production of P atoms may be expected in PH_3/H_2 systems. Such points should be checked experimentally. The role of vibrationally excited H_2 is not clear. This point must also be clarified since that is one of the most abundant species in plasma enhanced CVD processes.

8. Acknowledgements

The author is grateful to Professor Michael N. R. Ashfold of Bristol University and Dr. Yuri A. Mankelevich of Moscow State University for valuable discussions. He also acknowledges Professor Hideki Matsumura of Japan Advanced Institute of Science and Technology, who invited him to the research field of CVD.

Table 1. Apparent activation energies for the production of H atoms in catalytic decomposition of H_2.

Catalyst	Activation energy / kJ mol^{-1}	Ref.
W	~240	[45]
	190 [a]	[46]
	239	[21]
	217	[48]
	244	[51]
	210	[52]
Ta	177 [a]	[46]
	237	[47]
	~220	[49]
	~240	[44]
	105	[51]
Ir	295	[50]
Re	~230	[47]
Mo	228	[51]

[a] Gas constant, *R*, was multiplied to the originally reported value.

Table 2. Virtues and limitations of typical techniques to detect ground-state H atoms.

Technique	Excitation wavelength / nm	Direct determination of absolute densities	Spatial resolution	Sensitivity	Doppler width measurement	Effect of optical absorption	Multiphoton decomposition of molecular species	Effect of quenching	Effect of background signal	Ref.
RA [a]	121.6	possible and easy	not present [m]	medium	impossible	affected	not affected	not affected	affected a little	[51,84, 87-89]
VUV laser absorption [b]	121.6	possible and easy	not present	medium	possible but less accurate	affected	not affected	not affected	affected a little	[21,30, 50,52, 73, 90-94]
SR absorption [c]	121.6	possible and easy	not present	medium	possible but less accurate	affected	not affected	not affected	affected a little	[97]
VUV LIF [d]	121.6	possible	not present	high	possible	affected	not affected	affected a little	affected	[30,50, 90,91, 98]
Two-photon LIF [e]	243.1	impossible	present	high	possible and accurate	affected	affected	affected a little	affected	[30]
Three-photon LIF [f]	243.1 +656.3 or 486.1	impossible	present	medium	possible and accurate	not affected	affected	affected	affected	[67,101]
Two-photon LIF	205.1	possible	present	low	possible	not affected	affected	affected	affected	[21,30, 50,52, 54, 63-66, 70,76,

										82,94 103-119]
ASE [g]	205.1	impossible	present	low	possible	not affected	affected	not affected	not affected	[107, 114]
Two-photon polarization	243.1	possible	present	low	possible and accurate	not affected	affected	not affected	not affected	[124]
(2+1) REMPI [h]	243.1	impossible	present	medium	possible and accurate	not affected	affected	not affected	not affected	[44,47, 55,102, 125-127]
(2+1) REMPI with TOFMS [i]	243.1	impossible	present	very high	possible and accurate	not affected	affected	not affected	not affected	[57,58, 128]
(3+1) REMPI [j]	364.7	impossible	present	low	possible	not affected	affected a little	not affected	not affected	[45, 129]
THG [k]	364.7	impossible	present	low	impossible	affected a little	affected a little	not affected	not affected	[9,130]
TIMS [l]		impossible	not present	high	impossible	not affected at all	not affected at all	not affected at all	not affected at all	[48,49, 56,59, 68,71, 72,128, 137-141]

[a] resonance absorption

[b] vacuum-ultraviolet laser absorption

[c] synchrotron radiation absorption

[d] vacuum-ultraviolet laser-induced fluorescence

[e] two-photon laser-induced fluorescence

[f] two-color three-photon laser-induced fluorescence

[g] amplified spontaneous emission

[h] (2+1) resonance-enhanced multiphoton ionization

[i] (2+1) resonance-enhanced multiphoton ionization with time-of-flight mass spectrometry

[j] (3+1) resonance-enhanced multiphoton ionization

[k] third harmonic generation

[l] threshold ionization mass spectrometry

[m] spatial resolution can be improved using a small probe.[89]

Table 3. Steady-state densities of H atoms observed in catalytic and plasma decomposition of H_2.

	Material gas	Detection technique	$[H_2]$/Pa	Maximum [H] observed / cm^{-3}	Ref.
Catalytic decomposition	H_2	RA [a]	1.9	3×10^{11}	[51]
	H_2	VUV laser abs. [b] 2 photon LIF(205) [c]	1.1 7.5	7.0×10^{13} 1.8×10^{14}	[21]
	H_2	VUV laser abs. 2 photon LIF(205)	5.6	1.5×10^{14}	[94]
	H_2	VUV laser abs.	8.0	1.5×10^{12}	[73]
	H_2	VUV laser abs. 2 photon LIF(205) 2 photon LIF(243) [d] VUV LIF [e]	17	2.4×10^{12}	[30]
	H_2	VUV laser abs. 2 photon LIF(205) VUV LIF	17	1.2×10^{13}	[50]
	H_2	VUV laser abs. 2 photon LIF(205)	17	1.0×10^{13}	[52]
	H_2	SR abs. [f]	2.7×10^{3}	4×10^{15}	[97]
	H_2	2 photon LIF(205)	3.0×10^{3}	4.6×10^{15}	[103]
	H_2	2 photon LIF(205)	3.0×10^{3}	4.8×10^{15}	[104]
	CH_4(2%)/H_2	2 photon LIF(205)	4.0×10^{3}	1.2×10^{17}	[117]

	CH_4(0.5%)/Ar(0.5%)/H_2	TIMS [g] REMPI-TOF [h]	3.0×10^{3}	1.2×10^{15}	[128]
	CH_4(0.5%)/H_2	THG [i]	3.1×10^{3} 1.3×10^{4}	3×10^{15} 4×10^{15}	[9]
	CH_4(1%)/H_2	CARS [j] (H_2 density drop)	2.7×10^{3}	3.3×10^{16}	[167]
	CH_4(1%)/Ar(7%)/H_2	TIMS	2.7×10^{3}	4×10^{14}	[137]
	CH_4(0.4%)/Ar(11%)/H_2	TIMS	2.7×10^{3}	2×10^{14}	[138]
Plasma decomposition	Ar(4%)/H_2	OES [k]	40	4×10^{14}	[78]
	H_2	OES	60	7.0×10^{14}	[79]
	H_2	OES	267 533	1.3×10^{16} 3×10^{15}	[80]
	H_2	RA	1.3	1×10^{13}	[87]
	H_2	RA	1.3	2×10^{11}	[88]
	H_2	RA	10 25	2.6×10^{11} 8.5×10^{11}	[84]
	H_2	RA (micro probe)	1.3	1.2×10^{12}	[89]
	H_2	VUV laser abs. VUV LIF	530	2×10^{13}	[90]
	H_2	VUV laser abs. VUV LIF	230	2×10^{13}	[91]
	D_2(0.5%)/ H_2	VUV LIF	930	3.7×10^{12}	[98]
	D_2(0.5%)/ H_2	VUV laser abs.	1.6	6×10^{13}	[92]
	H_2	VUV laser abs.	1.6	2.4×10^{13}	[93]
	H_2,	2 photon LIF(205)	13	3×10^{11}	[63]

H_2	2 photon LIF(205)	400	8×10^{13}	[105]
H_2	2 photon LIF(205)	400	2.4×10^{14}	[106]
H_2	2 photon LIF(205)	27	1×10^{12}	[65]
H_2	2 photon LIF(205)	400	8×10^{14}	[70]
H_2	2 photon LIF(205) ASE [l]	133	1.4×10^{13}	[107]
H_2	2 photon LIF(205)	266	1.2×10^{13}	[109]
H_2	2 photon LIF(205)	40 720	2×10^{12} 4.0×10^{13}	[111]
H_2	2 photon LIF(205)	130	3.7×10^{15}	[112]
H_2	2 photon LIF(205)	50	2.0×10^{14}	[113]
H_2	2 photon LIF(205)	27	1×10^{12}	[76]
Ar(9%)/ H_2	2 photon LIF(205)	100	2.1×10^{15}	[118]
H_2	2 photon LIF(205)	13 130	5×10^{13} 3×10^{14}	[119]
H_2	2 photon polar. [m]	750 970	5×10^{13} 6×10^{13}	[124]
H_2	THG	2.1×10^{3}	2×10^{14}	[130]
H_2	TIMS	40	5×10^{12}	[139]
H_2	TIMS	40	3×10^{13}	[71]
H_2	TIMS	800	2.0×10^{15}	[141]
SiH_4(10%)/H_2	TIMS	200	5×10^{10}	[68]

[a] resonance absorption

[b] vacuum-ultraviolet laser absorption

[c] two-photon laser-induced fluorescence at 205 nm

[d] two-photon laser-induced fluorescence at 243 nm

[e] vacuum-ultraviolet laser-induced fluorescence

[f] synchrotron radiation absorption

[g] threshold ionization mass spectrometry

[h] (2+1) resonance-enhanced multiphoton ionization at 243 nm with time-of-flight mass spectrometry

[i] third harmonic generation

[j] coherent anti-Stokes Raman scattering

[k] optical emission spectroscopy

[l] amplified spontaneous emission

[m] two-photon polarization spectroscopy

Table 4. Rotational and vibrational distributions of H_2 in hot-wire excitation.

Detection technique	Filament temperature	Total pressure	Filament/ detection zone distance	Rotational temperature	v=1/v=0 ratio (Vibrational temperature)	Ref.
CARS	2820 K	2.7 kPa	0.65 cm	1590 K	<0.05 (<2000 K)	[167]
H^- monitoring	1770 K	6.7 Pa		700 K [a]	0.002 [a] (960 K)	[153]
VUV absorption	2270-2760 K	2.7 kPa	0.3 cm	1300 K	0.01 (1300 K)	[171]
			0.1 cm	1500 K	0.02 (1500 K)	
CARS	2400 K	3.0 kPa (0.5% CH_4)	0.5 cm	1000 K	0.01 (1300 K)	[128]
			0.1 cm	1600 K	0.06 (2130 K)	
CARS	2700 K	670 Pa	5 cm	1030 K	0.009 (1270 K)	[169]
		2.7 kPa	5 cm	1200 K	0.015 (1420 K)	

[a] values with walls covered with W.

Table 5. Rotational and vibrational distributions of H_2 in plasma excitation.

Detection technique	Electric power / Voltage / Current	Total pressure	Rotational temperature	v=1/v=0 ratio (Vibrational temperature)	Ref.
CARS	90 V, 10 A	5.5 Pa	530 K	0.082 (2390 K)	[165]
REMPI	100 V, 10 A	1.2 Pa	390 K	0.090 (2480 K)	[129]
3+1 REMPI	100V, 5A	1 Pa		0.083 (2400 K)	[172]
	100V, 30A			0.11 (2700 K)	
CARS	0.5 W cm^{-3}	200 Pa	600 K	0.22 (3980 K)	[168]
	2.0 W cm^{-3}	1.07 kPa	800 K	0.14 (3000 K)	
CARS	<200 W	200 Pa	540 K [a]	0.17 [a] (3400 K)	[170]
		1.07 kPa	610 K [a]	0.11 [a] (2700 K)	

[a] values in inductive-capacitive RF discharge plasma

References

[1] H. Matsumura, *Jpn. J. Appl. Phys.* **1998,** *37,* 3175.

[2] R.E.I. Schropp, *Thin Solid Films* **2009,** *517,* 3415.

[3] H. Matsumura, K. Ohdaira, *Thin Solid Films* **2009,** *517,* 3420.

[4] J. E. Butler, Y. A. Mankelevich, A. Cheesman, J. Ma, M. N. R. Ashfold, *J. Phys.: Condensed Matter* **2009,** *21,* 364201.

[5] J. W. Sutherland, M.-C. Su, J. V. Michael, *Int. J. Chem. Kinet.* **2001,** *33,* 669.

[6] M. G. Bryukov, I. R. Slagle, V. D. Knyazev, *J. Phys. Chem. A* **2001,** *105,* 3107.

[7] W. L. Hsu, *J. Vac. Sci. Technol. A* **1988,** 6, 1803.

[8] T. R. Anthony, *Vacuum* **1990,** *41,* 1356.

[9] L. L. Connell, J. W. Fleming, H.-N. Chu, D. J. Vestyck, Jr., E. Jensen, J. E. Butler, *J. Appl. Phys.* **1995,** *78,* 3622.

[10] M. N. R. Ashfold P. W. May, J. R. Petherbridge, K. N. Rosser, J. A. Smith, Y. A. Mankelevich, N. V. Suetin, *Phys. Chem. Chem. Phys.* **2001,** *3,* 3471.

[11] M. Frenklach, H. Wang, *Phys. Rev. B* **1991,** *43,* 1520.

[12] A. Izumi, T. Ueno, Y. Miyazaki, H. Oizumi, I. Nishiyama, *Thin Solid Films* **2008**, *516*, 853.

[13] A. Matsuda, *Thin Solid Films* **1999,** *337,* 1.

[14] A. Matsuda, *Jpn. J. Appl. Phys.* **2004,** *43,* 7909.

[15] A. Matsuda, *J. Non-Cryst. Solids* **2004,** *338-340,* 1.

[16] K. Tankala, T. DebRoy, *J. Appl. Phys.* **1992,** *72***,** 712.

[17] N. L. Arthur, L. A. Miles, *J. Chem. Soc. Faraday Trans.* **1997,** *93,* 4259.

[18] T. Ito, K. Fukunaga, T. Fujiwara, S. Nonomura, *Thin Solid Films* **2003,** *430,* 33.

[19] A. Heya, A. Masuda, H. Matsumura, *Appl. Phys. Lett.* **1999,** *74,* 2143.

[20] A. Heya, A. Masuda, H. Matsumura, *J. Non-Cryst. Solids* **2000,** *266-269,* 619.

[21] H. Umemoto, K. Ohara, D. Morita, Y. Nozaki, A. Masuda, H. Matsumura, *J. Appl. Phys.* **2002,** *91,* 1650.

[22] B. P. Swain, T. K. G. Rao, M. Roy, J. Gupta, R. O. Dusane, *Thin Solid Films* **2006,** *501*, 173.

[23] A. H. Mahan, A. C. Dillon, L. M. Gedvilas, D. L. Williamson, J. D. Perkins, *J. Appl. Phys.* **2003,** *94*, 2360.

[24] Q. Wang, S. Ward, L. Gedvilas, B. Keyes, E. Sanchez, S. Wang, *Appl. Phys. Lett.* **2004,** *84*, 338.

[25] F. Liu, S. Ward, L. Gedvilas, B. Keyes, B. To, Q. Wang, E. Sanchez, S. Wang, *J. Appl. Phys.* **2004,** *96*, 2973.

[26] A. Heya, T. Niki, M. Takano, Y. Yonezawa, T. Minamikawa, S. Muroi, S. Minami, A. Izumi, A. Masuda, H. Umemoto, H. Matsumura, *Jpn. J. Appl. Phys.* **2004,** *43*, L1546.

[27] T. Fujinaga, M. Takagi, M. Hashimoto, S. Asari, K. Saito, *Thin Solid Films* **2008,** *516,* 615.

[28] H. Umemoto, T. Morimoto, M. Yamawaki, Y. Masuda, A. Masuda, H. Matsumura, *Thin Solid Films* **2003,** *430,* 24.

[29] S.G. Ansari, H. Umemoto, T. Morimoto, K. Yoneyama, A. Izumi, A. Masuda, H. Matsumura, *Thin Solid Films* **2006,** *501,* 31.

[30] H. Umemoto, M. Moridera, *J. Appl. Phys.* **2008,** *103,* 034905.

[31] H. Umemoto, S. G. Ansari, T. Morimoto, S. Setoguchi, H. Uemura, H. Matsumura, *Thin Solid Films* **2008,** *516*, 829.

[32] M. Sommer, F. W. Smith, *J. Mater. Res.* **1990,** *5,* 2433.

[33] H. Toyoda, M. A. Childs, K. L. Menningen, L. W. Anderson, J. E. Lawler, *J. Appl. Phys.* **1994,** *75,* 3142.

[34] H. Okabe, *Photochemistry of Small Molecules,* John-Wiley & Sons, New York, 1978.

[35] R. J. Cvetanović, *Prog. React. Kinet.* **1964,** *2,* 39.

[36] W.H. Breckenridge, H. Umemoto, *Adv. Chem. Phys.* **1982,** *50,* 325.

[37] J. Larjo, J. Walewski, R. Hernberg, *Appl. Phys. B* **2001,** *72,* 455.

[38] W. Juchmann, J. Luque, J. B. Jeffries, *Appl. Opt.* **2005,** *44,* 6644.

[39] S. Johansson, T. R. Gull, H. Hartman, V. S. Letokhov, *Astronomy Astrophys.* **2005,** *435,* 183.

[40] D. K. Bhattacharyya, L.-Y. C. Chiu, *J. Chem. Phys.* **1977,** *67,* 5727.

[41] I. Langmuir, *J. Am. Chem. Soc.* **1912,** *34,* 860.

[42] I. Langmuir, G. M. J. Mackay, *J. Am. Chem. Soc.* **1914,** *36,* 1708.

[43] I. Langmuir, *J. Am. Chem. Soc.* **1915,** *37,* 417.

[44] D. W. Comerford, J. A. Smith, M. N. R. Ashfold, Y. A. Mankelevich, *J. Chem. Phys.* **2009,** *131,* 044326.

[45] F. G. Celii, J. E. Butler, *Appl. Phys. Lett.* **1989,** *54,* 1031.

[46] T. Otsuka, M. Ihara, H. Komiyama, *J. Appl. Phys.* **1995,** *77,* 893.

[47] S. A. Redman, C. Chung, K. N. Rosser, M. N. R. Ashfold, *Phys. Chem. Chem. Phys.* **1999,** *1,* 1415.

[48] W. Zheng, A. Gallagher, *Surf. Sci.* **2006,** *600,* 2207.

[49] W. Zheng, A. Gallagher, *Thin Solid Films* **2008,** *516,* 929.

[50] H. Umemoto, H. Kusanagi, K. Nishimura, M. Ushijima, *Thin Solid Films* **2009,** *517,* 3446.

[51] K. Abe, M. Ida, A. Izumi, S. Terashima, T. Sudo, Y. Watanabe, Y. Fukuda, *Thin Solid Films* **2009,** *517,* 3449.

[52] M. Yamamoto, T. Maruoka, A. Kono, H. Horibe, H. Umemoto, *Appl. Phys. Express* **2010,** *3,* 026501.

[53] H.L. Duan, S.F. Bent, *Thin Solid Films* **2005,** *485,* 126.

[54] M. Chenevier, J.C. Cubertafon, A. Campargue, J.P. Booth, *Diam. Relat. Mater.* **1994,** *3,* 587.

[55] J. A. Smith, M. A. Cook, S. R. Langford, S. A. Redman, M. N. R. Ashfold, *Thin Solid Films* **2000,** *368,* 169.

[56] J. Doyle, R. Robertson, G. H. Lin, M. Z. He, A. Gallagher, *J. Appl. Phys.* **1988,** *64,* 3215.

[57] S. Tange, K. Inoue, K. Tonokura, M. Koshi, *Thin Solid Films* **2001,** *395,* 42.

[58] K. Tonokura, K. Inoue, M. Koshi, *J. Non-Cryst. Solids* **2002,** *299-302,* 25.

[59] W. Zheng, A. Gallagher, *Thin Solid Films* **2006,** *501,* 21.

[60] H. Umemoto, K. Ohara, D. Morita, T. Morimoto, M. Yamawaki, A. Masuda, H. Matsumura, *Jpn. J. Appl. Phys.* **2003,** *42,* 5315.

[61] H. Umemoto, H. Kusanagi, *Open Chem. Phys. J.* **2009,** *2,* 32.

[62] H. Umemoto, T. Morimoto, M. Yamawaki, Y. Masuda, A. Masuda, H. Matsumura, *J. Non-Cryst. Solids* **2004,** *338-340,* 65.

[63] T. Kajiwara, K. Takeda, H. J. Kim, W. Z. Park, T. Okada, M. Maeda, K. Muraoka, M. Akazaki, *Jpn. J. Appl. Phys.* **1990,** *29,* L154.

[64] W. Z. Park, M. Tanigawa, T. Kajiwara, K. Muraoka, M. Masuda, T. Okada, M. Maeda, A. Suzuki, A. Matsuda, *Jpn. J. Appl. Phys.* **1992,** *31,* 2917.

[65] K. Tachibana, *Jpn. J. Appl. Phys.* **1994,** *33,* 4329.

[66] U. Czarnetzki, K. Miyazaki, T. Kajiwara, K. Muraoka, T. Okada, M. Maeda, A. Suzuki, A. Matsuda, *J. Vac. Sci. Technol. A* **1994,** *12,* 831.

[67] K. Miyazaki, T. Kajiwara, K. Uchino, K. Muraoka, T. Okada, M. Maeda, *J. Vac. Sci. Technol. A* **1997,** *15,* 149.

[68] P. Horvath, A. Gallagher, *J. Appl. Phys.* **2009,** *105,* 013304.

[69] D. L. Baulch, C. J. Cobos, R. A. Cox, C. Esser, P. Frank, Th. Just, J. A. Kerr, M. J. Pilling, J. Troe, R. W. Walker, J. Warnatz, *J. Phys. Chem. Ref. Data* **1992,** *21,* 411.

[70] A. D. Tserepi, T. A. Miller, *J. Appl. Phys.* **1994,** *75,* 7231.

[71] P. Kae-Nune, J. Perrin, J. Jolly, J. Guillon, *Surf. Sci.* **1996,** *360,* L495.

[72] J. Perrin, M. Shiratani, P. Kae-Nune, H. Videlot, J. Jolly, J. Guillon, *J. Vac. Sci. Technol. A* **1998,** *16,* 278.

[73] S.G. Ansari, H. Umemoto, T. Morimoto, K. Yoneyama, A. Masuda, H. Matsumura, M. Ikemoto, K. Ishibashi, *J. Vac. Sci. Technol. A* **2005,** *23,* 1728.

[74] H. F. Döbele, U. Czarnetzki, A. Goehlich, *Plasma Sources Sci. Technol.* **2000,** *9,* 477.

[75] J. Amorim, G. Baravian, J. Jolly, *J. Phys. D: Appl. Phys.* **2000,** *33,* R51.

[76] K. Tachibana, *Plasma Sources Sci. Technol.* **2002,** *11,* A166.

[77] H. F. Döbele, T. Mosbach, K. Niemi, V. Schulz-von der Gathen, *Plasma Sources Sci. Technol.* **2005,** *14,* S31.

[78] V. Schulz-von der Gathen, H. F. Döbele, *Plasma Chem. Plasma Process.* **1996,** *16,* 461.

[79] M. Abdel-Rahman, V. Schulz-von der Gathen, T. Gans, K. Niemi, H. F. Döbele, *Plasma Sources Sci. Technol.* **2006,** *15,* 620.

[80] W.-G. Wang, Y. Xu, Z.-C. Geng, Z.-W. Liu, A.-M. Zhu, *J. Phys. D: Appl. Phys.* **2007,** *40,* 4185.

[81] J. Ma, M. N. R. Ashfold, Y. A. Mankelevich, *J. Appl. Phys.* **2009,** *105,* 043302.

[82] A. Gicquel, M. Chenevier, Kh. Hassouni, A. Tserepi, M. Dubus, *J. Appl. Phys.* **1998,** *83,* 7504.

[83] J. C. Thomaz, J. Amorim, C. F. Souza, *J. Phys. D: Appl. Phys.* **1999,** *32,* 3208.

[84] S. Takashima, M. Hori, T. Goto, K. Yoneda, *J. Appl. Phys.* **2001,** *89,* 4727.

[85] A. C. G. Mitchell, M. W. Zemansky, *Resonance Radiation and Excited Atoms,* Cambridge University Press, London 1934.

[86] W. L. Wiese, J. R. Fuhr, *J. Phys. Chem. Ref. Data* **2009,** *38,* 565.

[87] S. Takashima, M. Hori, T. Goto, A. Kono, M. Ito, K. Yoneda, *Appl. Phys. Lett.* **1999,** *75,* 3929.

[88] S. Takashima, M. Hori, T. Goto, A. Kono, K. Yoneda, *J. Appl. Phys.* **2001,** *90,* 5497.

[89] S. Takahashi, S. Takashima, K. Yamakawa, S. Den, H. Kano, K. Takeda, M. Hori, *J. Appl. Phys.* **2009,** *106,* 053306.

[90] T. Kajiwara, M. Inoue, T. Okada, M. Maeda, K. Muraoka, M. Akazaki, *Jpn. J. Appl. Phys.* **1985,** *24,* 870.

[91] T. Kajiwara, M. Inoue, T. Okada, K. Muraoka, M. Akazaki, M. Maeda, *Rev. Sci. Instrum.* **1985,** *56,* 2213.

[92] D. Wagner, B. Dikmen, H. F. Döbele, *Rev. Sci. Instrum.* **1996,** *67,* 1800.

[93] D. Wagner, B. Dikmen, H. F. Döbele, *Plasma Sources Sci. Technol.* **1998,** *7,* 462.

[94] H. Umemoto, Y. Nozaki, M. Kitazoe, K. Horii, K. Ohara, D. Morita, K. Uchida, Y. Ishibashi, M. Komoda, K. Kamesaki, A. Izumi, A. Masuda, H. Matsumura, *J. Non-Cryst. Solids* **2002,** *299-302,* 9.

[95] G. C. Stutzin, A. T. Young, A. S. Schlachter, J. W. Stearns, K. N. Leung, W. B. Kunkel, G. T. Worth, R. R. Stevens, *Rev. Sci. Instrum.* **1988,** *59,* 1363.

[96] G. C. Stutzin, A. T. Young, A. S. Schlachter, J. W. Stearns, K. N. Leung, W. B. Kunkel, G. T. Worth, R. R. Stevens, *Rev. Sci. Instrum.* **1988,** *59,* 1479.

[97] M. A. Childs, K. L. Menningen, L. W. Anderson, J. E. Lawler, *J. Chem. Phys.* **1996,** *104,* 9111.

[98] K. Niemi, T. Mosbach, H. F. Döbele, *Chem. Phys. Lett.* **2002,** *367,* 549.

[99] R. Hilbig, R. Wallenstein, *Appl. Opt.* **1982,** *21,* 913

[100] G. Van Volkenburgh, T. Carrington, R. A. Young, *J. Chem. Phys.* **1973,** *59,* 6035.

[101] J. Deson, F. Haloua, C. Lalo, A. Rousseau, V. Veniard, *J. Phys. D: Appl. Phys.* **1994,** *27,* 2320**.**

[102] S. A. Redman, C. Chung, M. N. R. Ashfold, *Diam. Relat. Mater.* **1999,** *8,* 1383.

[103] U. Meier, K. Kohse-Hoinghaus, L. Schafer, C.-P. Klages, *Appl. Opt.* **1990,** *29,* 4993.

[104] L. Schäfer, C.-P. Klages, U. Meier, K. Kohse-Höinghaus, *Appl. Phys. Lett.* **1991,** *58,* 571.

[105] A. D. Tserepi, J. R. Dunlop, B. L. Preppernau, T. A. Miller, *J. Appl. Phys.* **1992,** *72,* 2638.

[106] A. D. Tserepi, J. R. Dunlop, B. L. Preppernau, T. A. Miller, *J. Vac. Sci. Technol. A* **1992,** *10,* 1188.

[107] J. Amorim, G. Baravian, M. Touzeau, J. Jolly, *J. Appl. Phys.* **1994,** *76,* 1487.

[108] K. Donnelly, D. P. Dowling, T. P. O'Brien, A. O'Leary, T. C. Kelly, R. Cheshire, K. F. Al-Assadi, W. G. Graham, T. Morrow, V. Kornas, V. Schulz-von der Gathen, H. F. Döbele, *Diam. Relat. Mater.* **1995,** *4,* 324.

[109] J. Amorim, G. Baravian, G. Sultan, *Appl. Phys. Lett.* **1996,** *68,* 1915.

[110] K. Miyazaki, T. Kajiwara, K. Uchino, K. Muraoka, T. Okada, M. Maeda, *J. Vac. Sci. Technol. A* **1996,** *14,* 125.

[111] J. Amorim, J. Loureiro, G. Baravian, M. Touzeau, *J. Appl. Phys.* **1997,** *82,* 2795.

[112] B. N. Ganguly, P. Bletzinger, *J. Appl. Phys.* **1997,** *82,* 4772.

[113] L.Chérigier, U. Czarnetzki, D. Luggenhölscher, V. Schulz-von der Gathen, H. F. Döbele, *J. Appl. Phys.* **1999,** *85,* 696.

[114] J. Amorim, G. Baravian, *Opt. Comm.* **2001,** *192,* 277.

[115] J. Larjo, H. Koivikko, D. Li, R. Hernberg, *Appl. Opt.* **2001,** *40,* 765.

[116] M. Hertl, J. Jolly, G. Baravian, *J. Appl. Phys.* **2002,** *92,* 710.

[117] J. Larjo, H. Koivikko, K. Lahtonen, R. Hernberg, *Appl. Phys. B* **2002,** *74,* 583.

[118] X. R. Duan, H. Lange, A. Meyer-Plath, *Plasma Sources Sci. Technol.* **2003,** *12,* 554.

[119] J. Jolly, J.-P. Booth, *J. Appl. Phys.* **2005,** *97,* 103305.

[120] K. Niemi, V. Schultz-von der Gathen, H. F. Döbele, *J. Phys. D: Appl. Phys.* **2001,** *34,* 2330.

[121] M. L. Burshtein, B. P. Lavrov, V. N. Yakovlev, *Opt. Spectrosc.* **1987,** *62,* 729.

[122] J. Bittner, K. Kohse-Höinghaus, U. Meier, Th. Just, *Chem. Phys. Lett.* **1988,** *143,* 571.

[123] B. L. Preppernau, K. Pearce, A. Tserepi, E. Wurzberg, T. A. Miller, *Chem. Phys.* **1995,** *196,* 371.

[124] A. B. Gonzalo, M. I. de la Rosa, C. Pérez, S. Mar, K. Grützmacher, *Plasma Sources Sci. Technol.* **2004,** *13,* 150.

[125] Yu. A. Mankelevich, N. V. Suetin, J. A. Smith, M. N. R. Ashfold, *Diam. Relat. Mater.* **2002,** *11,* 567.

[126] J. A. Smith, J. B. Wills, H. S. Moores, A. J. Orr-Ewing, M. N. R. Ashfold, Y. A. Mankelevich, N. V. Suetin, *J. Appl. Phys.* **2002,** *92,* 672.

[127] D. W. Comerford, A. Cheesman, T. P. F. Carpenter, D. M. E. Davies, N. A. Fox, R. S. Sage, J. A. Smith, M. N. R. Ashfold, Y. A. Mankelevich, *J. Phys. Chem. A* **2006,** *110,* 2868.

[128] V. Zumbach, J. Schäfer, J. Tobai, M. Ridder, T. Dreier, T. Schaich, J. Wolfrum, B. Ruf, F. Behrendt, O. Deutschman, J. Warnatz, *J. Chem. Phys.* **1997,** *107,* 5918.

[129] J. H. M. Bonnie, P. J. Eenshuistra, H. J. Hopman, *Phys. Rev. A* **1988,** *37,* 1121.

[130] F. G. Celii, H. R. Thorsheim, J. E. Butler, L. S. Plano, J. M. Pinneo, *J. Appl. Phys.* **1990,** *68,* 3814.

[131] A. G. Löwe, A. T. Hartlieb, J. Brand, B. Atakan, K. Kohse-Höinghaus, *Combust. Flame* **1999,** *118,* 37.

[132] U. Czarnetzki, K. Miyazaki, T. Kajiwara, K. Muraoka, M. Maeda, H. F. Döbele, *J. Opt. Soc. Am. B* **1994,** *11,* 2155.

[133] K. Kotaki, Y. Sakurai, T. Arikawa, *J. Mass Spectrosc. Soc. Jpn.* **1995,** *43,* 351.

[134] J. A. Gray, R. Trebino, *Chem. Phys. Lett.* **1993,** *216,* 519.

[135] U. Czarnetzki, H. F. Döbele, *Rev. Sci. Instrum.* **1995,** *66,* 587.

[136] J. A. Gray, J. E. M. Goldsmith, R. Trebino, *Opt. Lett.* **1993,** *18,* 444.

[137] W. L. Hsu, *Appl. Phys. Lett.* **1991,** *59,* 1427.

[138] M. C. McMaster, W. L. Hsu, M. E. Coltrin, D. S. Dandy, *J. Appl. Phys.* **1994,** *76,* 7567.

[139] P. Kae-Nune, J. Perrin, J. Guillon, J. Jolly, *Plasma Sources Sci. Technol.* **1995,** *4,* 250.

[140] W.-G. Wang, Y. Xu, X.-F. Yang, W.-C. Wang, A.-M. Zhu, *Rapid Comm. Mass Spectrosc.* **2005,** *19,* 1159.

[141] W. G. Wang, Y. Xu, C. Dong, N. Z. Zhang, K. Y. Hou, H. Y. Li, *Euro. Phys. J. D: Atom. Molec. Opt. Plasma Phys.* **2008,** *50,* 257.

[142] A. Omont, *Prog. Quantum Electronics* **1977,** *5,* 69.

[143] T. Fujimoto, C. Goto, Y. Uetani, K. Fukuda, *Jpn. J. Appl. Phys.* **1985,** *24,* 875.

[144] A. Hirabayashi, Y. Nambu, T. Fujimoto, *Jpn. J. Appl. Phys.* **1986,** *25,* 1563.

[145] W. L. Gardner, *J. Vac. Sci. Technol. A* **1995,** *13*, 763.

[146] T. Morimoto, H. Umemoto, K. Yoneyama, A. Masuda, H. Matsumura, K. Ishibashi, H. Tawarayama, H. Kawazoe, *Jpn. J. Appl. Phys.* **2005,** *44,* 732.

[147] H. Miura, Y. Kuroki, K. Yasui, M. Takata, T. Akahane, *Thin Solid Films* **2008,** *516,* 503.

[148] H. Umemoto, H. Kusanagi, *J. Phys. D: Appl. Phys.* **2008,** *41,* 225505.

[149] H. Umemoto, *Appl. Phys. Exp.* **2010,** *3,* 076701.

[150] P. Berlemont, D. A. Skinner, M. Bacal, *Rev. Sci. Instrum.* **1993,** *64,* 2721.

[151] R. I Hall, I. Čadež, M. Landau, F. Pichou, C. Schermann, *Phys. Rev. Lett.* **1988,** *60,* 337.

[152] P. J. Eenshuistra, J. H. M. Bonnie, J. Los, H. J. Hopman, *Phys. Rev. Lett.* **1988,** *60,* 341.

[153] C. Schermann, F. Pichou, M. Landau, I. Čadež, R. I Hall, *J. Chem. Phys.* **1994,** *101,* 8152.

[154] G. C. Light, *J. Chem. Phys.* **1978,** *68,* 2831.

[155] G. P. Glass, B. K. Chaturvedi, *J. Chem. Phys.* **1981,** *75,* 2749.

[156] W. Meier, G. Ahlers, H. Zacharias, *J. Chem. Phys.* **1986,** *85,* 2599.

[157] J. Arnold, T. Dreier, D. W. Chandler, *Chem. Phys.* **1989,** *133,* 123.

[158] R. A. Sultanov, D. Guster, *Chem. Phys. Lett.* **2006,** *428,* 227.

[159] T.-G. Lee, N. Balakrishnan, R. C. Forrey, P. C. Stancil, G. Shaw, D. R. Schultz, G. J. Ferland, *Astrophys. J.* **2008,** *689,* 1105.

[160] T. A. Brunner, D. Pritchard, *Adv. Chem. Phys.* **1982,** *50,* 589.

[161] T. Mosbach, H.-M. Katsch, H. F. Döbele, *Phys. Rev. Lett.* **2000,** *85,* 3420.

[162] Th. Mosbach, V. Schulz-von der Gathen, H. F. Döbele, *Contrib. Plasma Phys.* **2002,** *42,* 650.

[163] G. C. Stutzin, A. T. Young, A. S. Schlachter, K. N. Leung, W. B. Kunkel, *Chem. Phys. Lett.* **1989,** *155,* 475.

[164] G. C. Stutzin, A. T. Young, H. F. Döbele, A. S. Schlachter, K. N. Leung, W. B. Kunkel, *Rev. Sci. Instrum.***1990,** *61,* 619.

[165] M. Péalat, J-P. E. Taran, M. Bacal, F. Hillion*, J. Chem. Phys.* **1985,** *82,* 4943.

[166] S. O. Hay, W. C. Roman, M. B. Colket, *J. Mater. Res.* **1990,** *5,* 2387.

[167] K.-H. Chen, M.-C. Chuang, C. M. Penney, W. F. Banholzer, *J. Appl. Phys.* **1992,** *71,* 1485.

[168] V. A. Shakhatov, O. De Pascale, M. Capitelli, K. Hassouni, G. Lombardi, A. Gicquel, *Phys. Plasmas* **2005,** *12,* 023504.

[169] H. Umemoto, S.G. Ansari, H. Matsumura, *J. Appl. Phys.* **2006,** *99,* 043510.

[170] V. A. Shakhatov, O. A. Gordeev, *Opt. Spectrosc.* **2007,** *103,* 468.

[171] K. L. Menningen, M. A. Childs, L. W. Anderson, J. E. Lawler, *Rev. Sci. Instrum.* **1996,** *67,* 1546.

[172] P. J. Eenshuistra, A. W. Kleyn, H. J. Hopman, *Europhys. Lett.* **1989,** *8,* 423.

[173] J. Arnold, T. Bouché, T. Dreier, J. Wichmann, J. Wolfrum, *Chem. Phys. Lett.* **1993,** *203,* 283.

[174] M. M. Audibert, C. Joffrin, J. Ducuing, *Chem. Phys. Lett.* **1974,** *25,* 158.

[175] M.-M. Audibert, R. Vilaseca, J. Lukasik, J. Ducuing, *Chem. Phys. Lett.* **1975,** *31,* 232.

[176] T. G. Kreutz, J. Gelfand, R. B. Miles, H. Rabitz, *Chem. Phys.* **1988,** *124,* 359

[177] M. Cacciatore, G. D. Billing, *J. Phys. Chem.* **1992,** *96,* 217.

[178] D. R. Flower, E. Roueff, *J. Phys. B* **1998,** *31,* 2935.

[179] V. A. Zenevich, G. D. Billing, G. Jolicard, *Mol. Phys.* **2000,** *98,* 1691.

[180] S. K. Pogrebnya, D. C. Clary, *Chem. Phys. Lett.* **2002,** *363,* 523.

[181] J. E. Dove, H. Teitelbaum, *Chem. Phys.* **1974,** *6,* 431.

[182] D. R. Flower, E. Roueff, *J. Phys. B* **1998,** *31,* L955.

[183] O. Dobis, S. W. Benson, *J. Phys. Chem. A* **2002,** *106,* 4403.

[184] Y. A. Mankelevich, M. N. R. Ashfold, D. W. Comerford, J. Ma, J. C. Richley, *Thin Solid Films,* in press.

Figure captions

Fig. 1. Crystalline volume fraction in hydrogenated microcrystalline silicon plotted against the substrate temperature. The hydrogen-dilution ratios were 19, 9, and 4 from top to bottom.
Reprinted from *J. Non-Cryst. Solids* **2004,** *338-340,* 1.

Fig. 2. Dependence of the decomposition efficiency of NH_3 on H_2 flow rate in the presence (circles) and in the absence (triangles) of SiH_4. The flow rates of NH_3 and SiH_4 were 10 and 5 sccm, respectively.
Reprinted from *Thin Solid Films* **2006,** *501*, 31.

Fig. 3. Tungsten catalyst temperature, T_{cat}, dependence of the H atom density between 1300 and 2200 K in the presence of 5.6 Pa of H_2 measured by a two-photon laser-induced fluorescence technique (○) and by a vacuum ultraviolet absorption technique (●). The absolute values were determined by a vacuum ultraviolet absorption technique.
Reprinted from *J. Appl. Phys.* **2002,** *91,* 1650.

Fig. 4. Energy level diagram for the detection of H atoms.
[a] resonance absorption and vacuum-ultraviolet laser absorption at 121.6 nm
[b] one-photon laser-induced fluorescence following the excitation at 121.6 nm
[c] two-photon laser-induced fluorescence following the excitation at 243.2 nm
[d] three-photon laser-induced fluorescence following the excitation at 243.2 and 656.3 nm
[e] two-photon laser-induced fluorescence and amplified spontaneous emission following the excitation at 205.1 nm
[f] (2+1) resonance-enhanced multiphoton ionization
[g] (3+1) resonance-enhanced multiphoton ionization
[h] third harmonic generation

Fig. 5 Vacuum ultraviolet absorption spectra of H atoms produced by catalytic decomposition of H_2. The W catalyst temperatures were 1270, 1320, 1370, and 1410 K from top to bottom. The pressure and the flow rate of H_2 were 5.6 Pa and 150 sccm, respectively.

Reprinted from *J. Appl. Phys.* **2002,** *91,* 1650.

Fig. 6. Absolute H-atom densities measured at various H_2 pressures. Closed circles represent the results for catalytic decomposition, while open circles represent the results for plasma decomposition.

Fig. 7. Q-branch CARS spectra of H_2 activated on a heated W filament. (a) H_2 pressure of 1.3 kPa without heating the filament; (b) H_2 pressure of 2.7 kPa with heating the filament up to 2700 K. The distance between the filament and the detection zone was 5 cm.

Reprinted from *J. Appl. Phys.* **2006,** *99,* 043510.

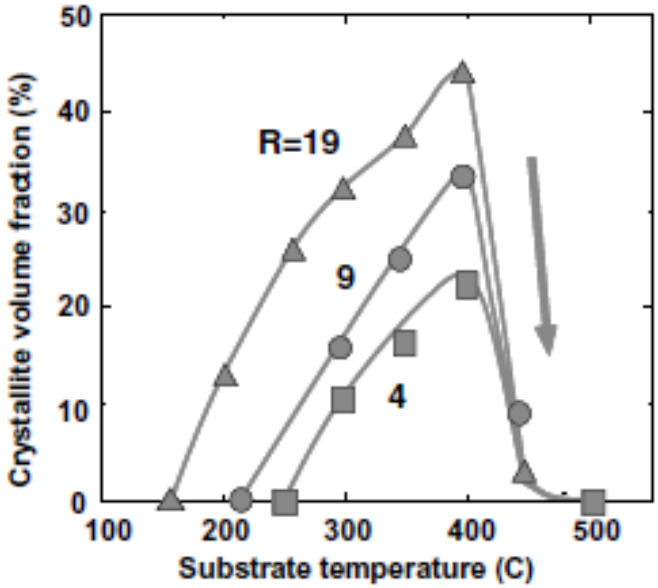

Fig. 1. (H. Umemoto)

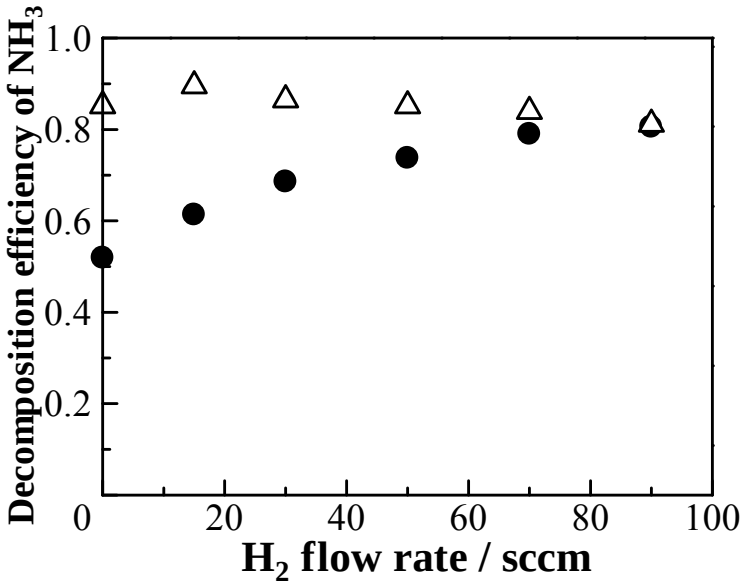

Fig. 2. (H. Umemoto)

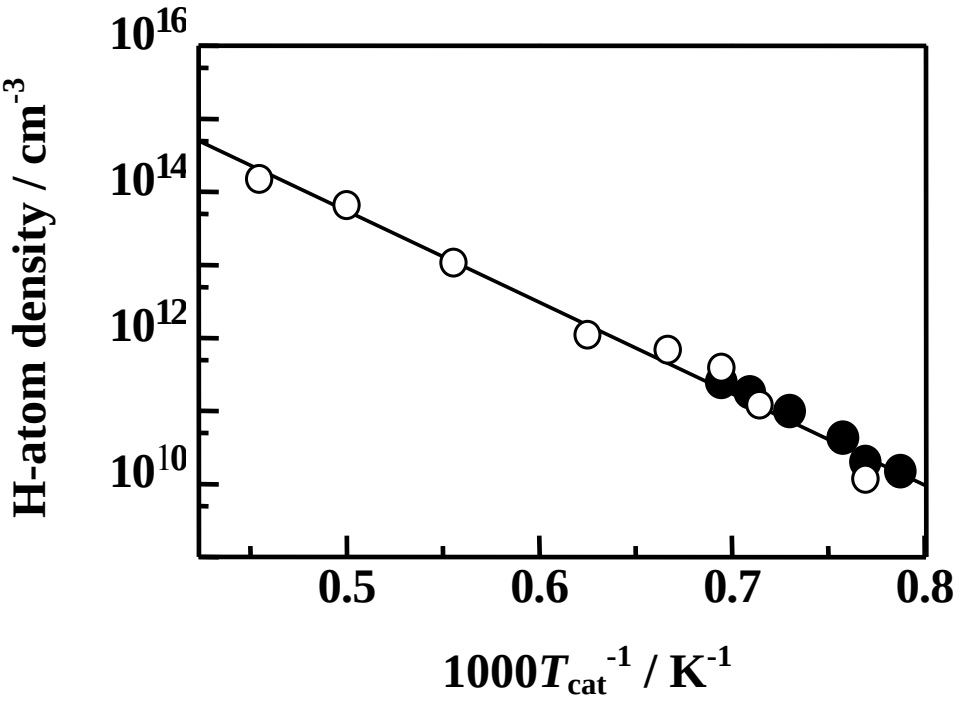

Fig. 3. (H. Umemoto)

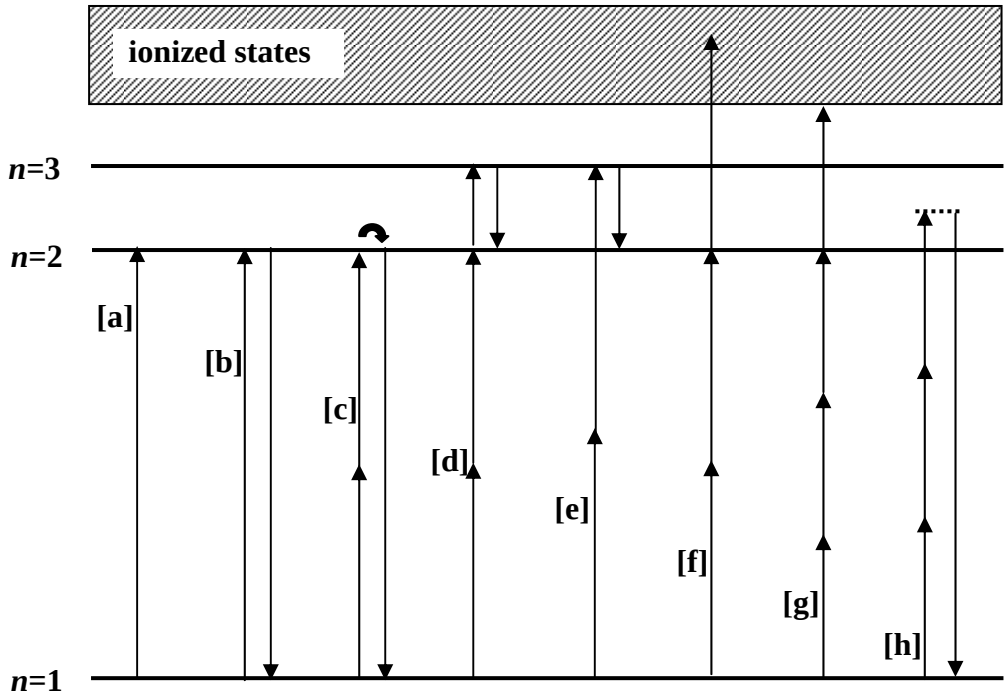

Fig. 4. (H. Umemoto)

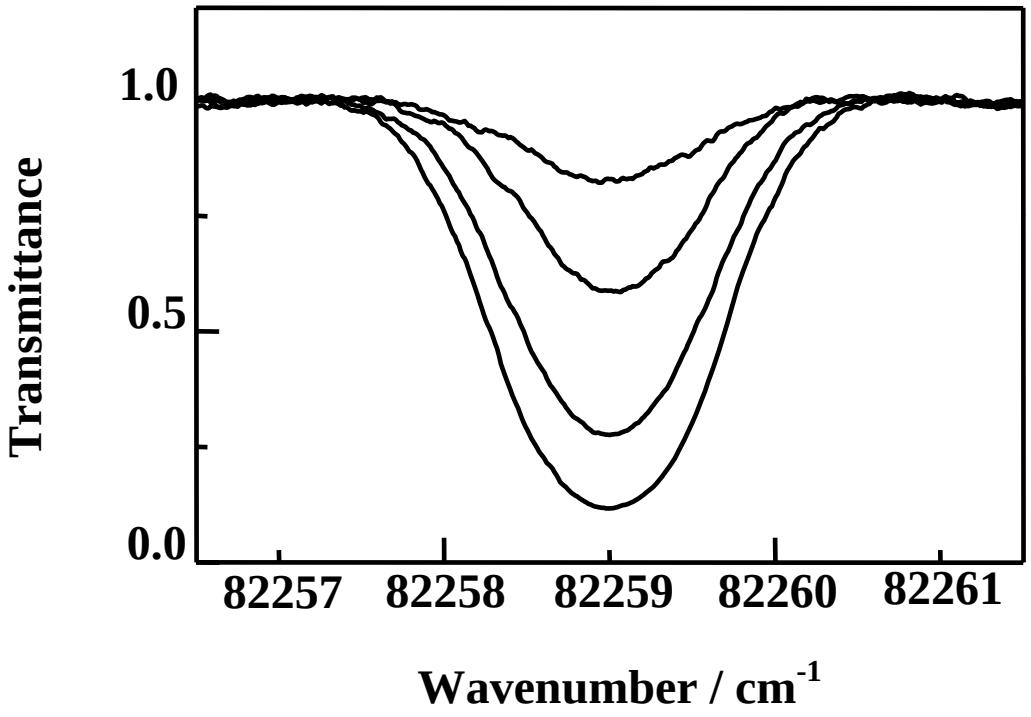

Fig. 5. (H. Umemoto)

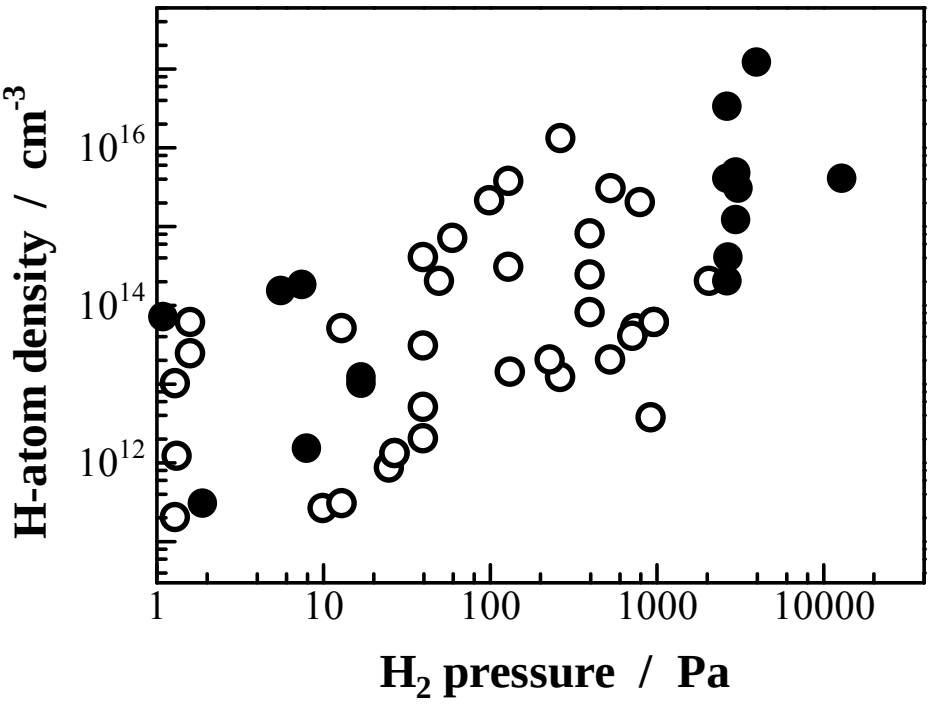

Fig. 6. (H. Umemoto)

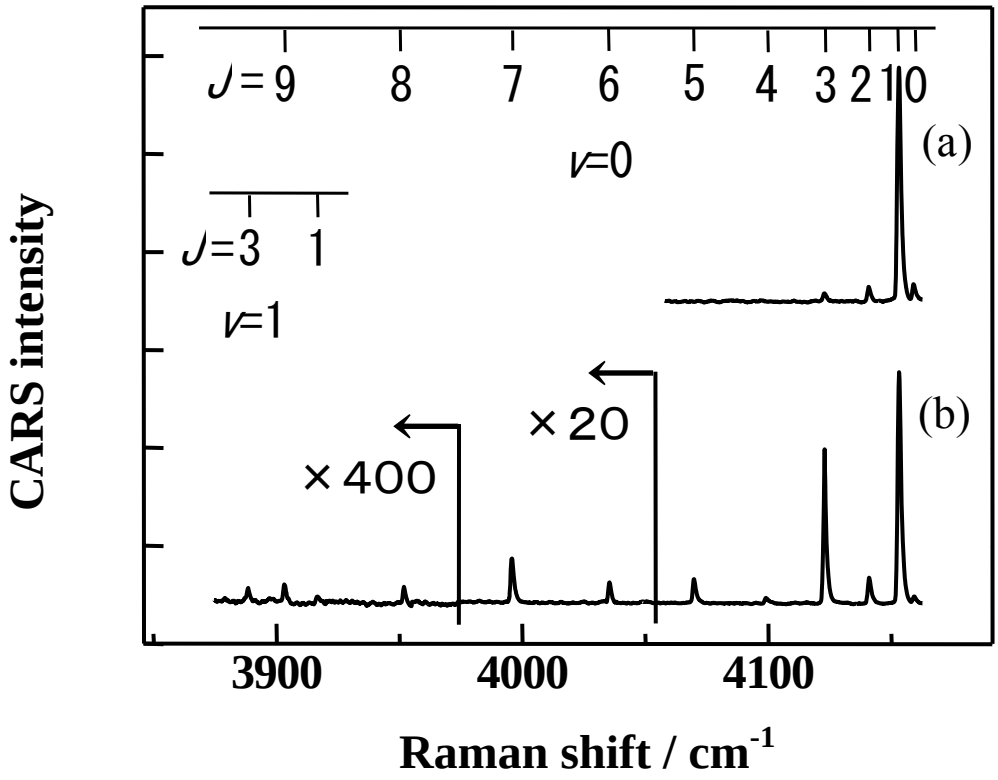

Fig. 7. (H. Umemoto)